Chapter 11

Control of Hierarchical Structure of Crystalline Nanofibers Based on the Cooperative Phenomena of Functional Molecular Group as the Target of Expression of New Physical Properties: Creation of Molecular Conductors and Enhancement of Thixotropic Ability

Manami Iizuka, Rie Yamato and Atsuhiro Fujimori

Additional information is available at the end of the chapter

http://dx.doi.org/10.5772/63701

Abstract

In this chapter, a study on two kinds of examples of functional nanofibers has been introduced. In the first section, the formation of nanofiber morphology at a mesoscopic scale and molecular level stacking of a tetrathiafulvalene (TTF) derivative with a chiral group were investigated by the one-dimensional growth method in interfacial molecular films. Monomolecular films of a TTF derivative with a chiral borneol group display a two-dimensional phase transition at the air/water interface. The formation of nanonetwork domains is attributed to the organized aggregation of the TTF derivatives, which is a result of strong intermolecular interactions. In the second section, the formation of nanofiber morphology at a mesoscopic scale and molecular level packing of an amphiphilic diamide derivative with two hydrocarbons were investigated by the in interfacial molecular films. It has found that the growth of this nanofiber morphology is encouraged by the application of the epitaxial growth in the spin-cast film with 1 wt% layered silicate having long hydrocarbons. As mention above, it is found that mesoscopic morphological formation of super-hierarchical structure of the nanofibers having a crystalline arrangement at Å level can be induced conductivity and the thixotropy at macroscopic level.

Keywords: crystalline nanofiber, TTF derivative, diamide derivative with two hydrocarbons, thixotropic ability, one-dimensional growth

1. Morphological transition of a conductive molecular organization with non-covalent from nanonetwork to nanofiber

1.1. Introduction

Although the synthesis of the Langmuir–Blodgett (LB) film was first reported by Blodgett in 1934 [1], this technique has attracted a lot of attention in recent years, following its application in the formation of two-dimensional lamellae in linear polymers [2]. While there is a long history of development of this technique beginning with the studies on the optical and electronic properties of the LB films by Khun et al. [3, 4], direct observation of the folding of polymer chains in LB films using atomic force microscopy was a significant milestone, which revealed the phenomenon of "morphogenesis at the interface" [5, 6]. For the several examples of "morphogenesis at the interface," the formation of nanofibers [7], nanowires [8, 9], nanospheres [10], nanocoils [11], nanoribbons [12], sea-island structures [13, 14], rods [15], gyroids [16], lamellae [17], and honeycombs [18] are noteworthy. Simultaneous control of the mesoscopic morphology (at the sub-micron level) of a non-covalent molecular organization, along with control of the molecular arrangement and packing structure (at the sub-nanometer level), is essential for the construction of next-generation quantum devices and medical materials. In other words, the molecular arrangement and morphology need to be controlled at different dimensional scales.

In this chapter, the formation of a nanofiber morphology at the mesoscopic scale and the molecular level stacking of a tetrathiafulvalene (TTF) derivative with a chiral group were investigated by the method of one-dimensional molecular film growth (**Figure 1(a)**). The fabrication of a nanometer-scale thin film having a fibril texture, which was achieved by incorporating a phenyl group in the TTF derivatives, has been reported previously [19]. However, the strong interactions between the molecules, which is a consequence of the competing forces of π–π interactions (of TTFs and phenyl rings) and hydrogen-bonding (of urethane bonding units), inhibited accurate morphological control. Therefore, in our previous study, we attempted to substitute the phenyl ring with the bulky and chiral borneol group [20], in order to minimize these strong intermolecular interactions. However, since TTF derivatives containing borneol groups are amorphous, top-down fabrication of thin films and control of the molecular arrangement were quite difficult.

Organized molecular films [21] have been developed as potential candidates for the synthesis of biomimetic models [22] and molecular electronic devices [23, 24], which are of considerable technological interest [25–29]. In addition to the interaction of lipids and proteins with hydrocarbons, various amphiphiles containing functional groups (including π- and *d*-electron systems), and polymerizable groups have been synthesized to obtain monolayer assemblies with well-defined molecular arrangements [30]. Therefore, this technology could potentially provide an effective means for attaining hierarchically precise and regular structures.

http://dx.doi.org/10.5772/63701

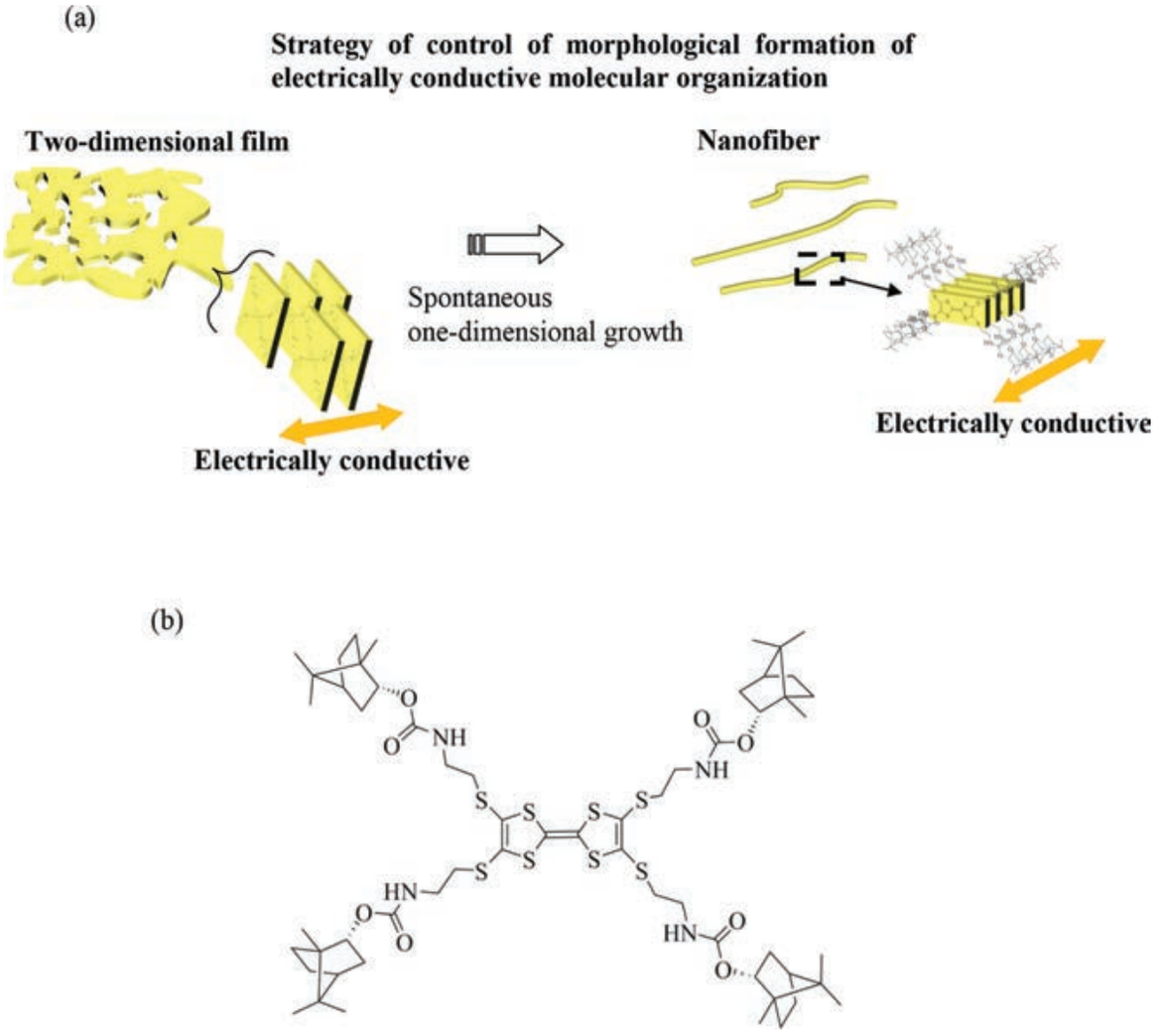

Figure 1. (a) Formation of nanofiber morphology at mesoscopic scale and molecular level stacking and (b) chemical structure of TTF-4Bor.

In the present chapter, a new, conducting, four-armed amphiphilic compound (a TTF derivative with chiral borneol groups (TTF-4Bor, **Figure 1(b)** [20]) was synthesized. The monolayer behavior, molecular arrangement, and surface morphology of organized molecular films of TTF-4Bor were investigated by analysis of the surface pressure–area (π–A) isotherms, in-plane and out-of-plane X-ray diffraction (XRD) profiles, and atomic force microscopy (AFM) images. Further, morphogenesis was encouraged by applying the one-dimensional growth method to an LB film of TTF-4Bor in distilled water, under low surface pressure conditions. The size of the nanofibers thus obtained was controlled by variation of the subphase temperature. Since the internal structure of the mesoscopic nanofiber is comprised of stacked TTF planes at a molecular level, effective electrical conduction is expected along the direction of stacking.

1.2. Experimental section

1.2.1. Synthesis of TTF-4Bor (Scheme S1)

A three-necked flask with a stirrer was purged with nitrogen, followed by the addition of L(-)-borneol (compound **1**, 20.5 g, 1.33 mmol), 2-chloroethyl isocyanate (compound **2**, 16.8 g, 159 mmol), and anhydrous tetrahydrofuran (THF, 300 mL). To this, 24 drops of dibutyltin dilaurate were added, and the mixture was stirred overnight in an oil bath at 50°C. The solvent was then evaporated under reduced pressure, and the residue was purified by column chromatography over silica gel (chloroform/ethyl acetate = 9:1). The product (compound **3**) was obtained as a white solid with a yield of 84% (29.07 g, 112 mmol).

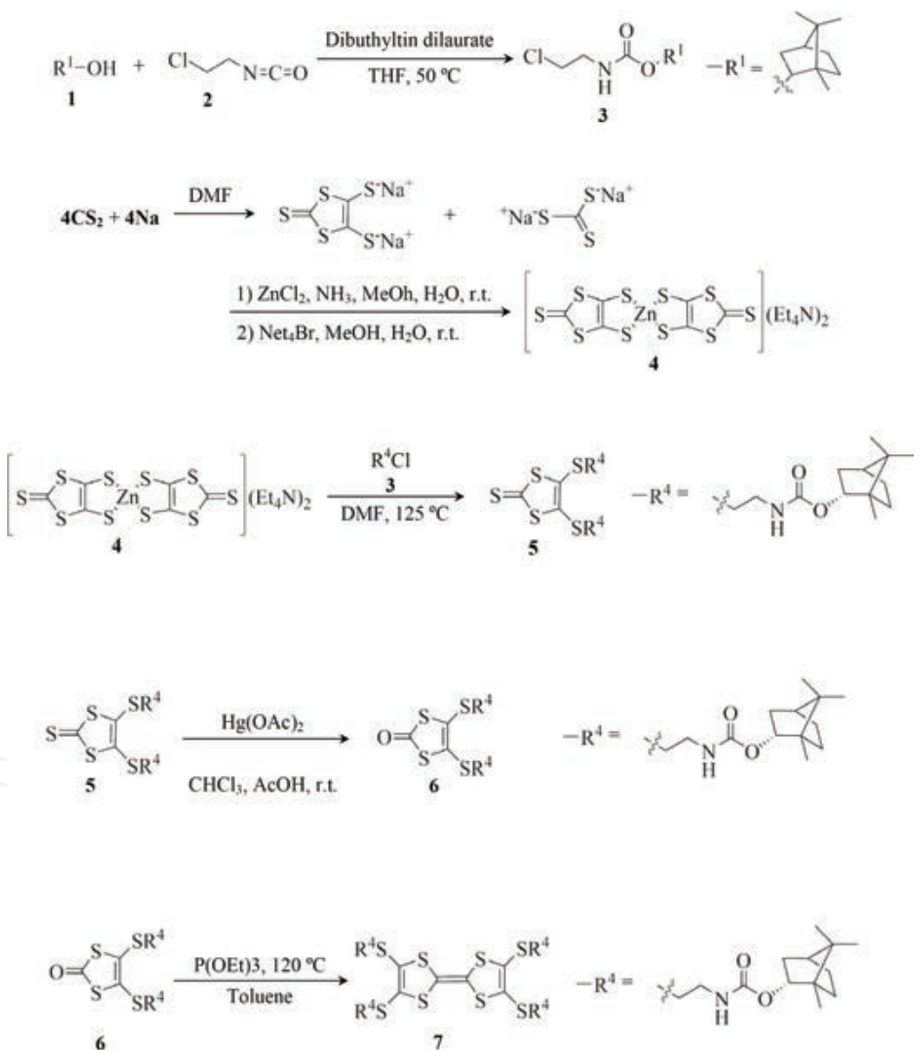

Scheme S1. Synthesis of TTF-4Bor.

Synthesis of Compound ***4***: To a 500-mL four-necked flask (with a stirrer, purged with nitrogen), shredded sodium (23.0 g, 1.00 mol) and carbon disulfide (180 mL, 3 mol) were added and stirred. Then, the four-necked flask was placed in an ice bath, and *N*,*N*-dimethylformamide

http://dx.doi.org/10.5772/63701

(DMF) (200 mL) was added in drops over 4 h through a dropping funnel. The mixture was removed from the ice bath, brought to room temperature, and stirred overnight. This was again cooled in an ice bath, and methanol (50 mL) was added slowly through a dropping funnel. The contents of the four-necked flask were then transferred to a 3 L conical flask, and a mixture of methanol (200 mL) and deionized water (250 mL) was added in drops, followed by the gradual addition of a solution of zinc chloride (20 g, 0.15 mol) in concentrated aqueous ammonia (500 mL). To this, a solution of tetraethylammonium bromide (106 g, 0.50 mol) in deionized water (500 mL) was added in drops over a period of 4 h (in two portions), and the mixture was stirred overnight. This was suction-filtered through a Kiriyama funnel, and the residue was washed with water (500 mL), isopropanol (200 mL), and diethyl ether (200 mL). This residue was dissolved in acetone, and the resulting solution was evaporated under reduced pressure. Red crystals of the desired product (compound **4**) were obtained with 97.6% yield (87.7 g, 0.12 mol).

*Synthesis of Compound **5***: In a 100-mL three-necked flask (with stirrer, purged with nitrogen), compound **4** (5.53 g, 7.70 mmol), compound **3** (10.00 g, 38.49 mmol), and DMF (90 mL) were added and stirred overnight in an oil bath at 125°C. Following concentration of the reaction mixture, the organic layer was extracted thrice with chloroform and distilled water, and dried using anhydrous magnesium sulfate. The magnesium sulfate was removed by filtration, and the filtrate was purified by column chromatography over silica gel (chloroform/ethyl acetate = 47:3). The desired product (compound **5**) was obtained as a yellow solid with 72.3% yield (7.19 g, 11.15 mmol).

*Synthesis of Compound **6***: To a 100-mL three-necked flask (with a stirrer, purged with nitrogen), compound **5** (1.00 g, 1.55 mmol), chloroform (9.70 mL), acetic acid (3.23 mL), and mercury acetate (II) (1.72 g, 4.13 mmol) were added, and this mixture was stirred overnight at room temperature. The mixture was then subjected to Celite filtration, and the filtrate was extracted thrice using chloroform and distilled water. The chloroform layer was washed thrice with a saturated aqueous sodium bicarbonate solution and dried over anhydrous magnesium sulfate. This mixture was purified by column chromatography over silica gel (ethyl acetate). The desired product (compound **6**) was obtained as a yellow solid with a yield of 84.1% (0.82 g, 1.3 mmol).

*Synthesis of Compound **7** (TTF-4Bor)*: In a 50-mL three-necked flask (with a stirrer, purged with nitrogen), a mixture of compound **6** (0.82 g, 1.30 mmol) and triethyl phosphite (1.5 mL) was heated in an oil bath at 120°C with stirring for half day. The triethyl phosphite was removed under reduced pressure, and the remaining solid was purified by column chromatography over silica gel (hexane/ethyl acetate = 3:2). The desired final product (compound **7**, TTF-4Bor, **Figure 1(b)**) was obtained as a yellow solid with a yield of 63% (0.51 g, 0.41 mmol). The chemical structure of this compound has been determined by NMR and IR spectroscopy previously [20].

1.2.2. Formation of monolayers of TTF-4Bor on the water surface

Monolayers were formed by spreading a toluene solution of TTF-4Bor ($\sim 1.0 \times 10^{-4}$ M) on the surface of distilled water (resistivity: approximately 18.2 MΩ cm). After evaporation of the toluene for 5 min, surface pressure–area (π–A) isotherms were recorded at compression speeds

ranging from 0.8 to 4.8 cm^2 min^{-1}. The air/water interface was kept at a constant temperature of 15°C by circulation of thermostated water around the trough. Measurement of the monolayer properties and LB film transfer were carried out in a USI-3-22 Teflon-coated LB trough (USI Instruments).

1.2.3. Study of the surface morphology and estimation of the molecular arrangement

The surface morphologies of the transferred films were observed using a scanning probe microscope (Atomic Force Microscopy, SII Nanotechnology, SPA300 with SPI-3800 probe station), and microfabricated rectangular Si cantilevers with integrated pyramidal tips, by applying a constant force of 1.4 N m^{-1}. In this chapter, AFM observations were carried out in the tapping mode. XRD samples were transferred onto a glass substrate by the LB method (20 layers, subphase temperature of 15°C, and surface pressures of 5 and 35 mN m^{-1}). The large spacing between the layers in the films was measured using an out-of-plane X-ray diffractometer (Rigaku, Rint-Ultima III, CuKα radiation, 40 kV, 30 mA) equipped with a graphite monochromator. The in-plane spacing of the two-dimensional lattice of the films was determined using an X-ray diffractometer with different geometrical arrangements [31, 32] (Bruker AXS, MXP-BX, CuKα radiation, 40 kV, 40 mA, a customized instrument) and equipped with a parabolic-graded multilayer mirror. The X-rays were incident at an angle of 0.2°, and the films were scanned at a speed of 0.05°/80 s, as a result of which the in-plane XRD measurements had monomolecular resolution.

1.3. Results and discussion

1.3.1. Monolayer behavior and surface morphology of TTF-4Bor

Figure 2 shows the π–A isotherms of a TTF-4Bor monolayer at the air/water interface at 15°C, along with the estimated collapse surface pressure and the limiting area. TTF-4Bor forms an expanded phase at low surface pressures and an extremely condensed phase at high surface pressures. These results indicate that the TTF-4Bor film undergoes a two-dimensional transition, from parallel to normal orientation on the water surface.

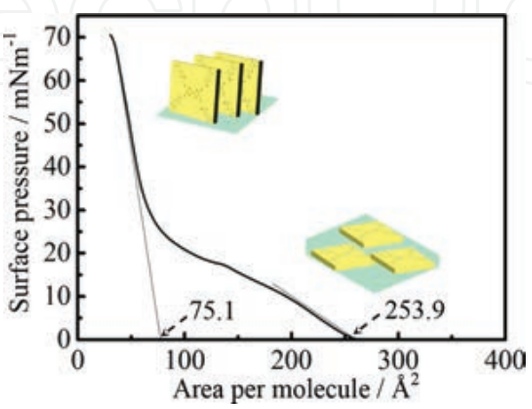

Figure 2. Surface pressure–area isotherm at the air/water interface for the TTF-4Bor monolayer.

http://dx.doi.org/10.5772/63701

Figure 3 shows the AFM images of LB monolayers of TTF-4Bor (Z-type) on mica, transferred at 35 and 10 mN m^{-1}. At low surface pressures, sparsely dotted nanodomains with a height of about 1 nm are observed, confirming the flat-on orientation of the molecular planes. In the high pressure regions, however, submicron network domains are formed, and the height information indicates that the conformation of the TTF derivatives is normal to the plane of the film. It has been suggested that the mesoscopic morphogenesis is attained by aggregation, which is based on the competition between the π–π interaction of the TTF molecular planes, and the strong interaction of hydrogen bonds between the urethane bonding sites. This hypothesis is supported by the infrared (IR) spectra (**Figure 3(c)**), which exhibit a shift of the band attributed to the carbonyl group toward lower wavenumbers, indicating the formation of hydrogen bonds [19, 20].

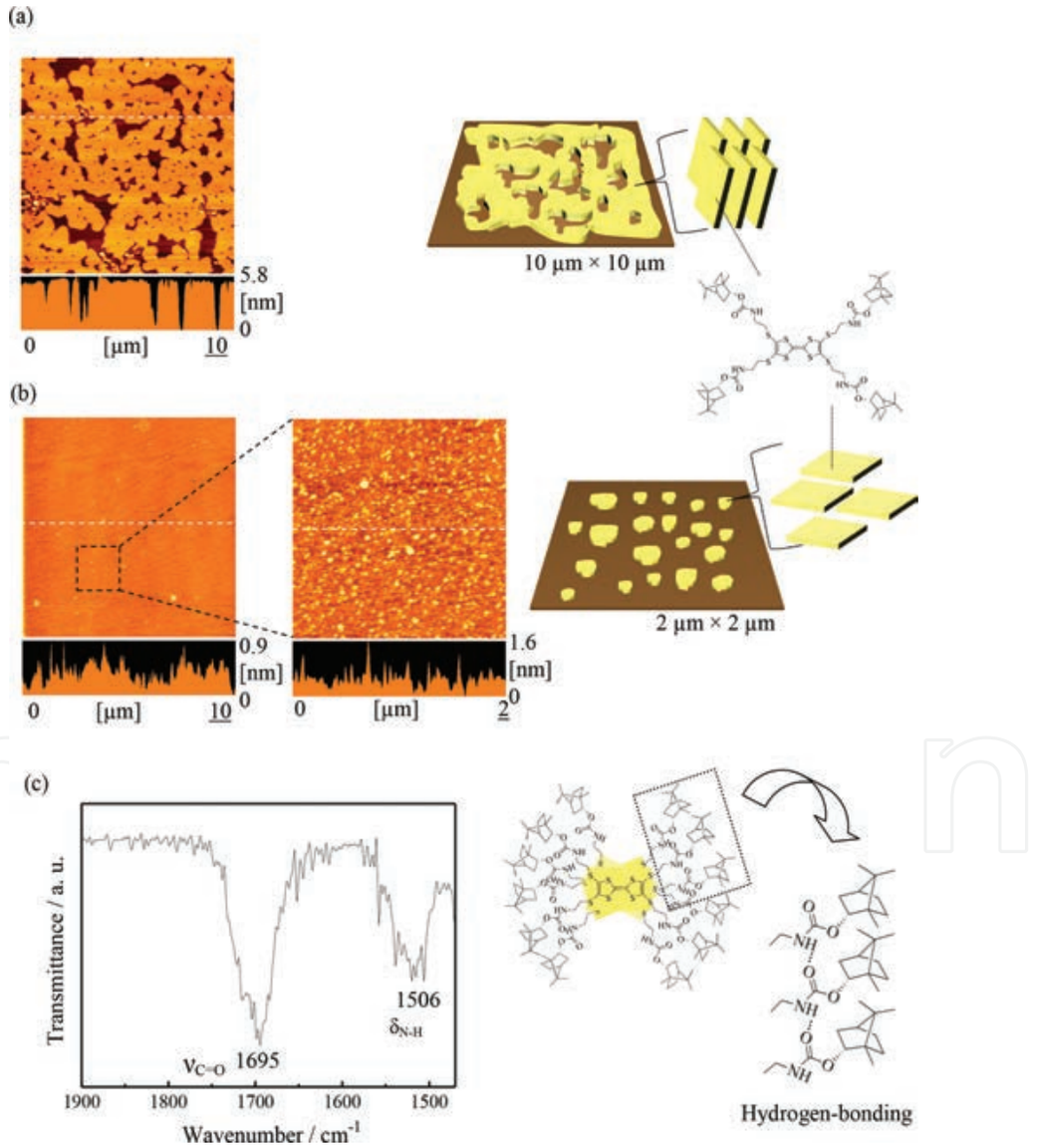

Figure 3. AFM images of Z-type monolayers of TTF-4Bor transferred at (a) 35 mN m^{-1} and (b) 10 mN m^{-1}; (c) IR spectra of LB multilayers of TTF-4Bor transferred at 35 mN m^{-1} on a CaF_2 substrate.

1.3.2. Molecular arrangement in organized molecular films of TTF-4Bor

In order to estimate the crystallinity and periodicity of the molecules in multilayers of TTF-4Bor, in-plane and out-of-plane XRD analyses of LB multilayers were carried out. In-plane XRD profiles of multilayers transferred at 35 and 10 mN m^{-1} are shown in **Figure 4**. This technique provides information regarding molecular arrangement at a sub-nanometer scale, and the internal fine structure of the mesoscopic morphology. At low surface pressures, a clear periodic structure was not observed, indicating that the film might be amorphous. On the other hand, in the LB multilayers formed at high surface pressures, a clear periodic structure with regular molecular packing was confirmed. The short spacing value of 4.1 Å appears to correspond to the stacking of the TTF molecular planes based on π–π interactions. A similar in-plane packing system based on π–π interactions, established by in-plane XRD, was reported in conducting organized molecular films of metal $(dmit)_2$ charge transfer complexes [33]. Dense stacking of molecular planes has been known to induce electrical conductivity along the direction of stacking.

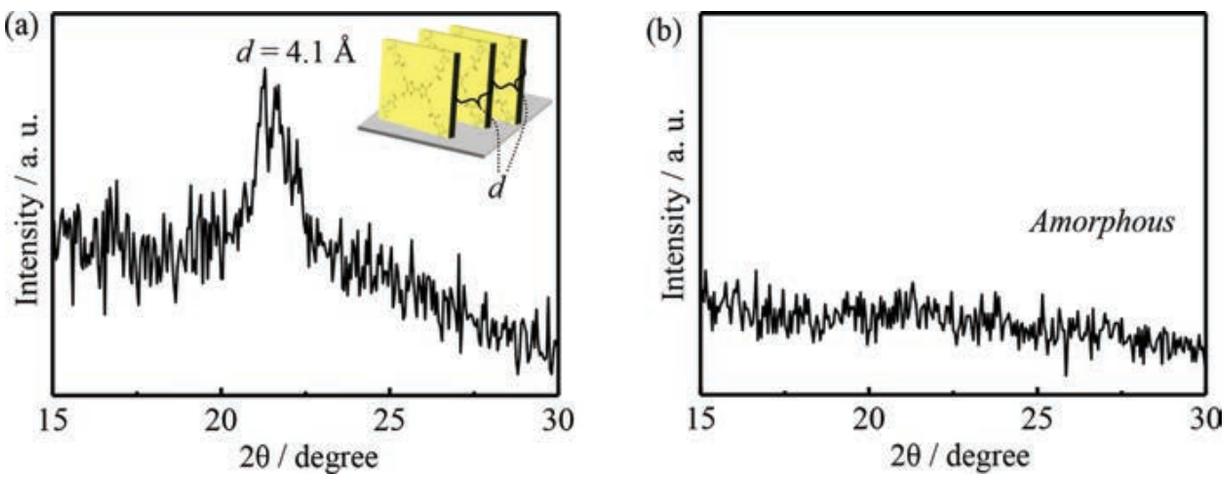

Figure 4. In-plane XRD profiles of LB multilayers (20 layers) of TTF-4Bor transferred at (a) 35 mN m^{-1} and (b) 10 mN m^{-1}.

Figure 5 shows the out-of-plane XRD profiles for LB multilayers (20 layers) of TTF-4Bor, transferred at 35 and 10 mN m^{-1}. In the multilayers fabricated under high surface pressure conditions, a $d_{0\,0\,1}$ layer corresponding to the end-on orientation of TTF-4Bor was observed along the *c*-axis. The formation of the highly regular layered structure is believed to have occurred during the transfer of the interfacial monomolecular film to a solid, by the LB method. At low surface pressures, a layer spacing of ~5 nm is observed in the multilayers, which exhibit molecular organization along with disorder in the *ab*-plane, and regularity along the *c*-axis. Therefore, rearrangement of the molecular groups is expected to take place during multilayer formation, along with a change in the conformation from flat-on to end-on, resulting in layered regularity in the *c*-direction. These results are summarized in **Figure 6**.

http://dx.doi.org/10.5772/63701

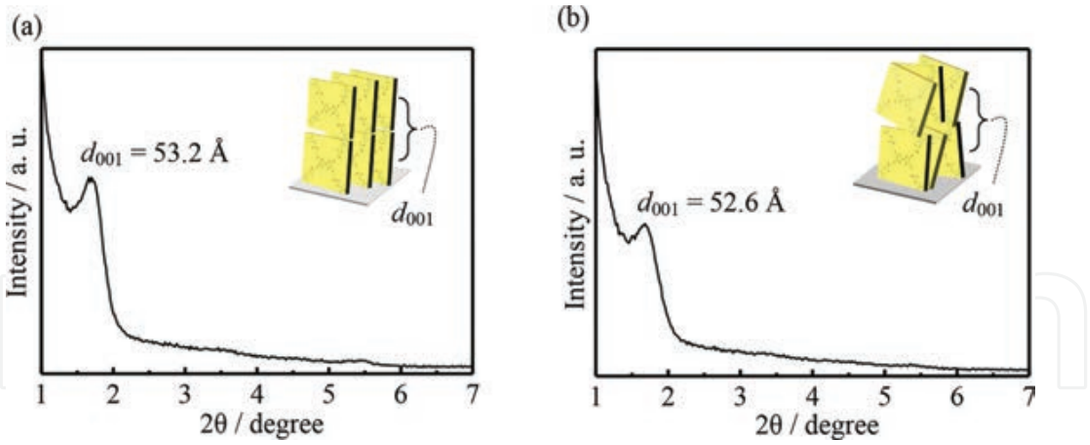

Figure 5. Out-of-plane XRD profiles of LB multilayers (20 layers) of TTF-4Bor transferred at (a) 35 mN m^{-1} and (b) 10 mN m^{-1}.

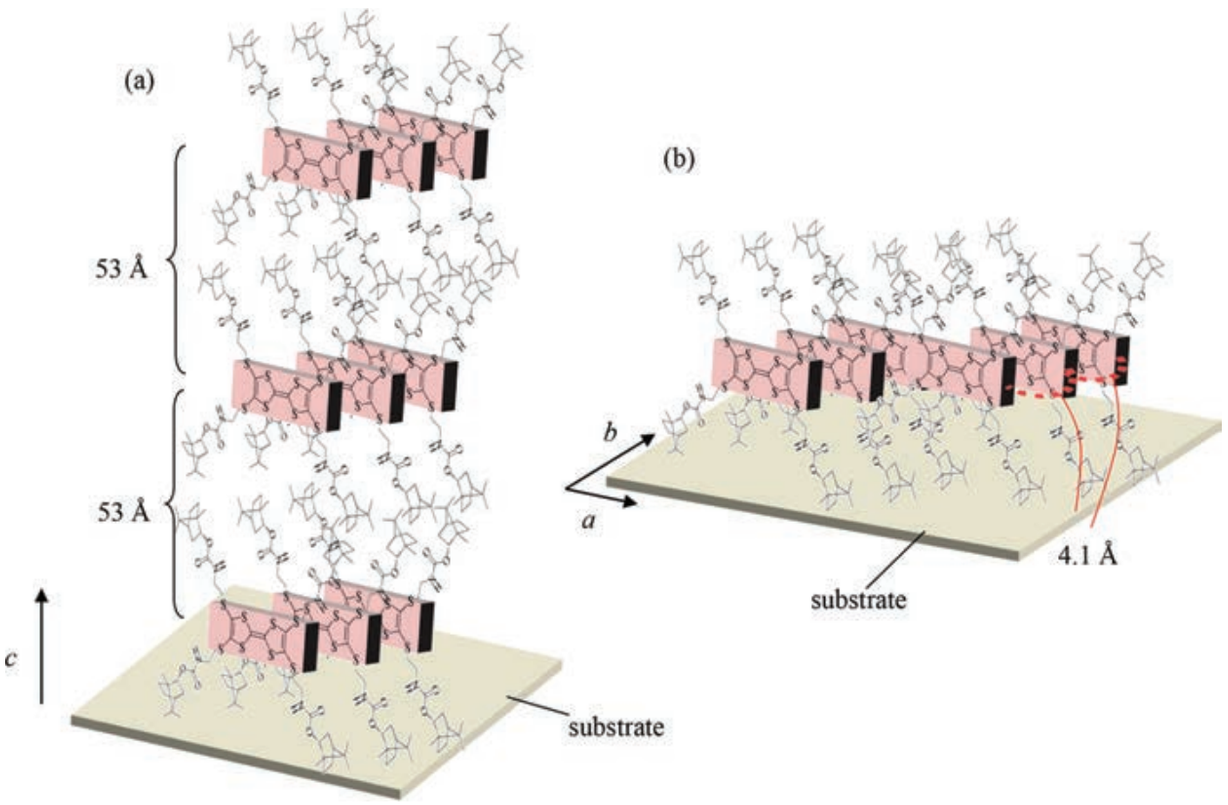

Figure 6. Schematic illustration of the (a) molecular arrangement of TTF-4Bor along the *c*-axis and (b) molecular stacking model of LB multilayers of TTF-4Bor in the *ab*-plane.

1.3.3. Morphological changes from a two-dimensional film to nanofibers of TTF-4Bor

At present, there are limitations in the ability to achieve one-dimensional growth of a nanofiber consisting of tightly stacked electrically conducting molecules. Although stacked conducting molecular planes are obtained at high surface pressures, morphologies at the mesoscopic scale

are too developed due to the strong forces of aggregation, with the presence of long-range order between molecules, as a result of the competitive effect of π–π interactions and hydrogen bonding. Hence, although the molecules cannot be arranged under low surface pressure conditions, the disordered molecular groups can be rearranged by multilayer formation, owing to their strong aggregation tendency. In this chapter, the technique of one-dimensional growth at the air/water interface was adopted, which involved transfer of the film at low surface pressures with reduction of the compression speed (by a factor of 8), inducing a spontaneous growth structure at the interface. **Figure 7** shows a comparison of the π–A isotherms, at different compression speeds (4.8 and 0.6 cm^2 min^{-1}), and a schematic illustration of molecular aggregation. The tendency to expand at low pressures and condense at higher pressures is conspicuous in the π–A isotherms measured at a low compression rate (0.6 cm^2 min^{-1}).

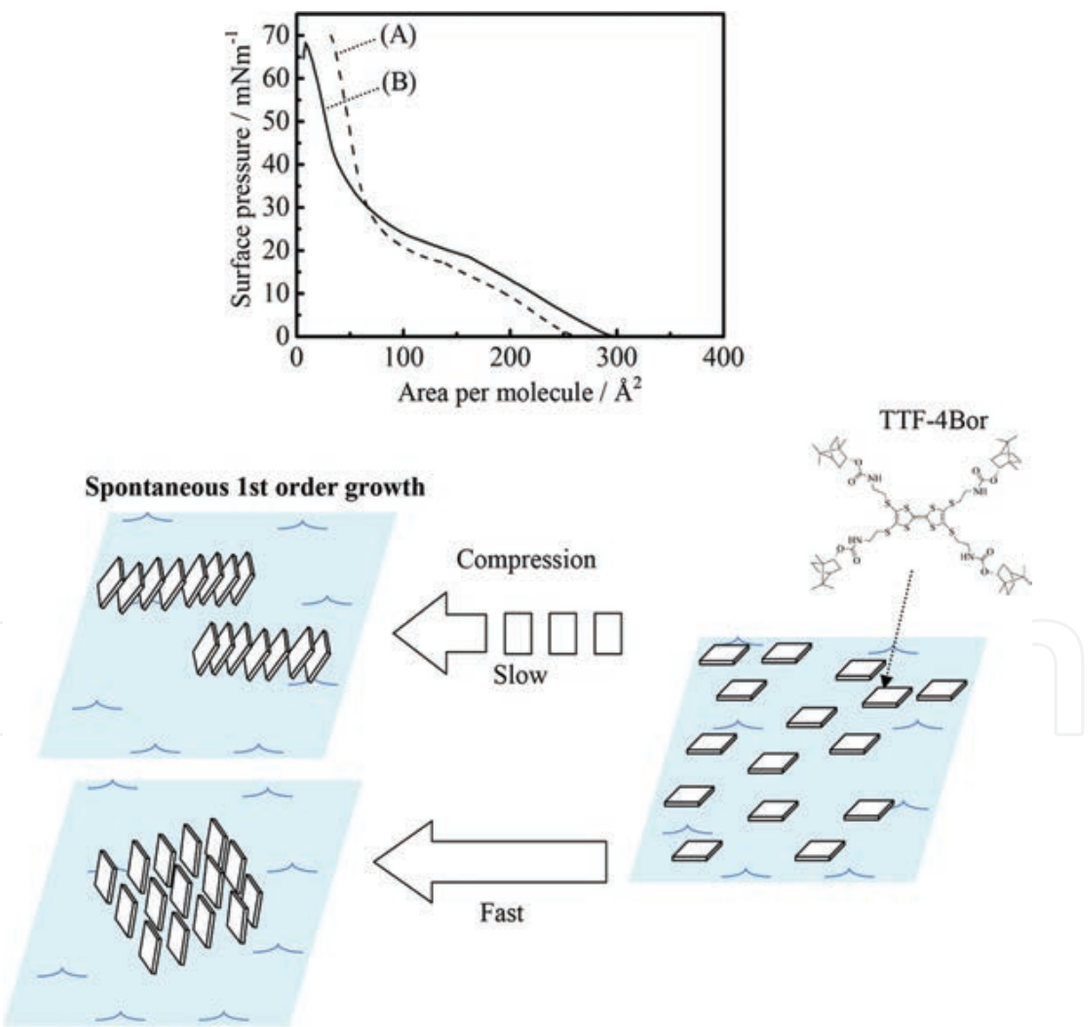

Figure 7. Surface pressure–area isotherms at different compression speeds (4.8 cm^2 min^{-1} [dashed line] and 0.6 cm^2 min^{-1} [solid line]) of monolayer of TTF-4Bor at the air/water interface.

http://dx.doi.org/10.5772/63701

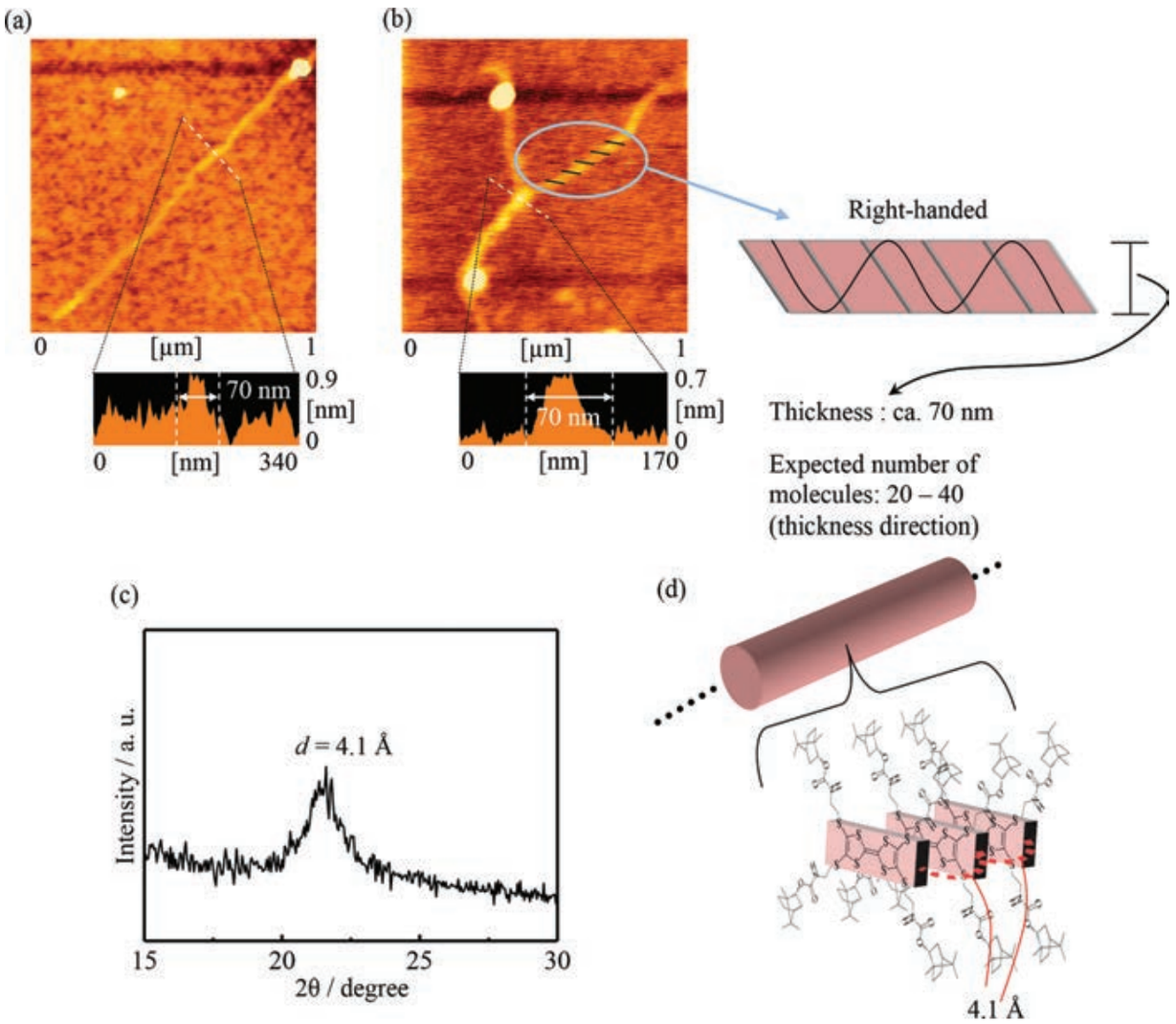

Figure 8. AFM images of Z-type monolayers of (a) nanofiber and (b) helical nanofiber forms of the one-dimensional growth TTF-4Bor. (c) In-plane XRD profiles of LB multilayers (20 layers) of TTF-4Bor (at 10 mN m^{-1} and compression speed 0.6 cm^2 min^{-1}), and (d) a schematic model for their molecular packing.

In **Figure 8**, AFM images of the Z-type monolayers of TTF-4Bor after one-dimensional growth are shown, along with the in-plane XRD profiles of multilayers of TTF-4Bor transferred at 10 mN m^{-1} with a compression speed of 0.6 cm^2 min^{-1}. In this system, there is a clear transition from a mesoscopic morphology to a nanofiber shape (thickness ~70 nm). While many of the nanofibers are linear (**Figure 8(a)**), some fibers exhibit a branching morphology (**Figure 8(b)**) and some others grew as a right-handed spiral. This morphological formation is expected to have occurred to minimize the steric hindrance from the four functional groups in the TTF derivative. This material exhibited circular dichroism (CD) for every adsorption band [20], and the Cotton effect centered around 380 and 530 nm was attributed to the helical dipole coupling between TTF rings through the formation of a network of hydrogen bonds [34–38]. In-plane

XRD reveals multilayers of these integrated nanofiber films, with the formation of stacked conducting molecular planes with a spacing of 4.1 Å (**Figures 8(c)** and **(d)**). It is expected that the promotion of spiral morphogenesis based on steric hindrance of chiral functional groups is dependent on the enhancement of the molecular mobility at the air/water interface. Therefore, the formation of nanofibers was studied at different subphase temperatures (**Figure 9**). It is seen that an increase in the subphase temperature results in an increase in the diameter of the fibers, rather than the formation of the helical structure, which could be due to an increase in the aggregation force between the molecules. The diameters of the nanofibers formed at 15, 20, and 25°C, are 70, 125, and 190 nm, respectively. From the π–A curves, these correspond to aggregates of 20–40 molecules at 15°C, 30–60 molecules at 20°C, and 50–90 molecules at 25°C. The nanofiber morphology was retained upon inclusion of 2,3,5,6-tetrafluoro-7,7,8,8-tetracyanoquinodimethane (F_4-TCNQ) acceptor molecules to this system at a molecular ratio of 1:1 (**Figure 10**). Since F_4-TCNQ is not amphiphilic, mixing it with the TTF derivative results in the formation of a charge transfer (CT) complex and interfacial nanofiber films. The retention of the nanofiber morphology after the inclusion of F_4-TCNQ is because the structural formation is related to the stacking arrangement of the TTF molecular planes, and first-order spontaneous growth of mesoscopic nanofibers. The CT complex exhibited a broad absorption band in the IR region (2500–3500 cm^{-1}), which was attributed to a CT between the electron-donating TTF and the electron-accepting F_4-TCNQ moieties [39–41]. **Figure 10** shows the color change of the solution to support the CT complex formation, and further, the AFM image and in-plane XRD profile also show evidences of maintaining of a mesoscopic fiber form and stacking of a conductive molecular plane. In addition, **Figure 10(c)** also shows UV spectrum of charge transfer complex of TTF-4Bor:F4-TCNQ = 1:1 in solution. Absorption band near 300 nm corresponds to the TTF-4Bor, and the band of 400 nm except the shoulder peak corresponding to F4-TCNQ. Absorption band at 700–800 nm corresponds to the anionic radical of the F4-TCNQ, and shoulder-shaped absorption band around 400 nm corresponds to the cationic radical of TTF [41]. From the above, the formation of a charge-transfer complex in solution is supported.

As detailed in this chapter, the amphiphilic TTF derivative with chiral borneol groups are closely packed in the nanofiber morphology at the air/water interface. Although the densely packed molecular arrangement is easily attained by standard film fabrication methods at high surface pressures, mesoscopic nanofiber morphology is obtained by spontaneous one-dimensional growth at the air/water interface (**Figure 11**). The dense stacking structure of these molecular planes induces electrical conduction, and nanofibrous morphogenesis can be deployed in quantum devices, medical applications, etc. It can be seen that the control of the mesoscopic morphology at the air/water interface provides several variations and possibilities in the chapter of molecular organization, such as helical morphogenesis and size control of nanofibers [42].

http://dx.doi.org/10.5772/63701

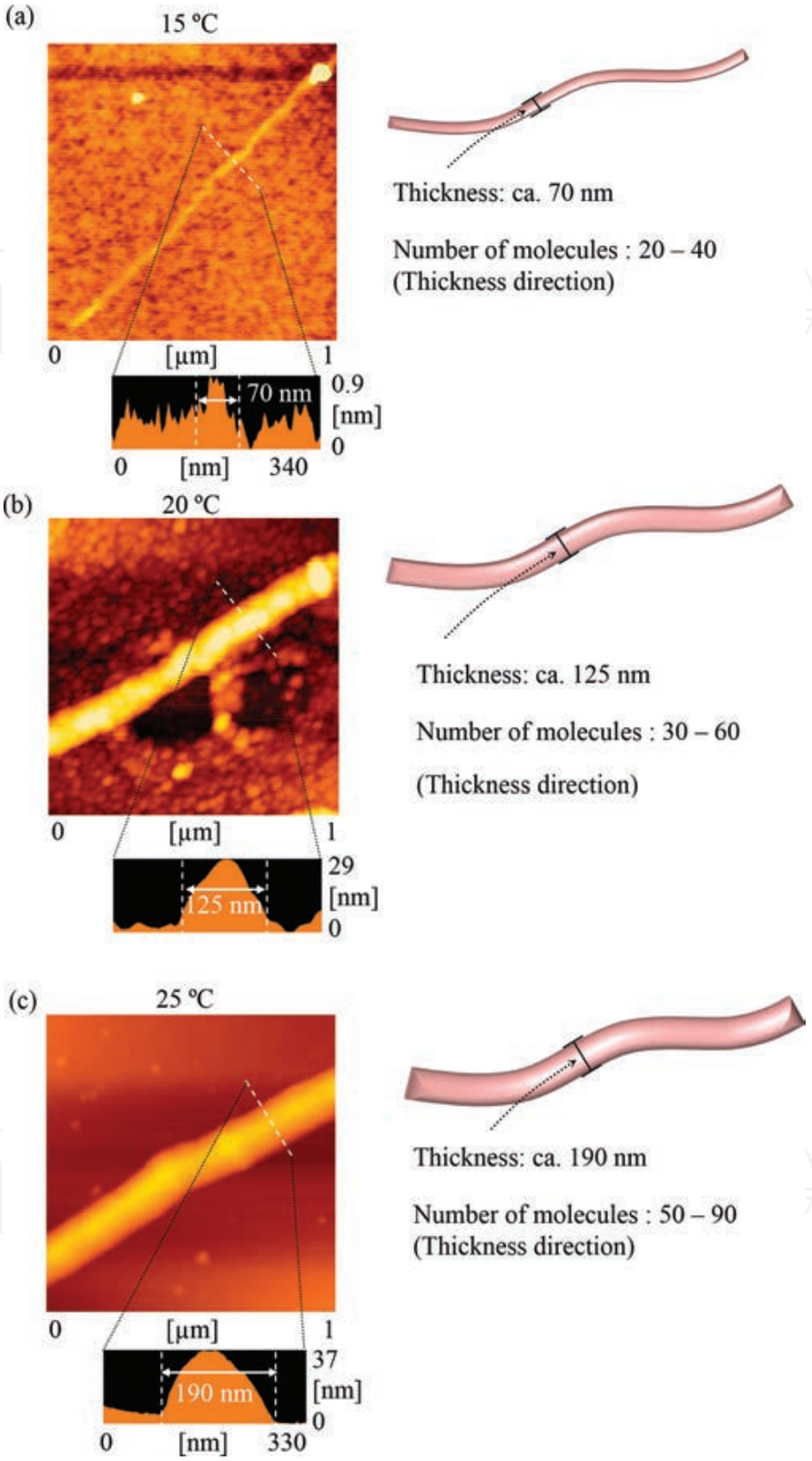

Figure 9. AFM images of Z-type monolayers of the one-dimensional growth of TTF-4Bor transferred at (a) 15°C, (b) 20°C, and (c) 25°C.

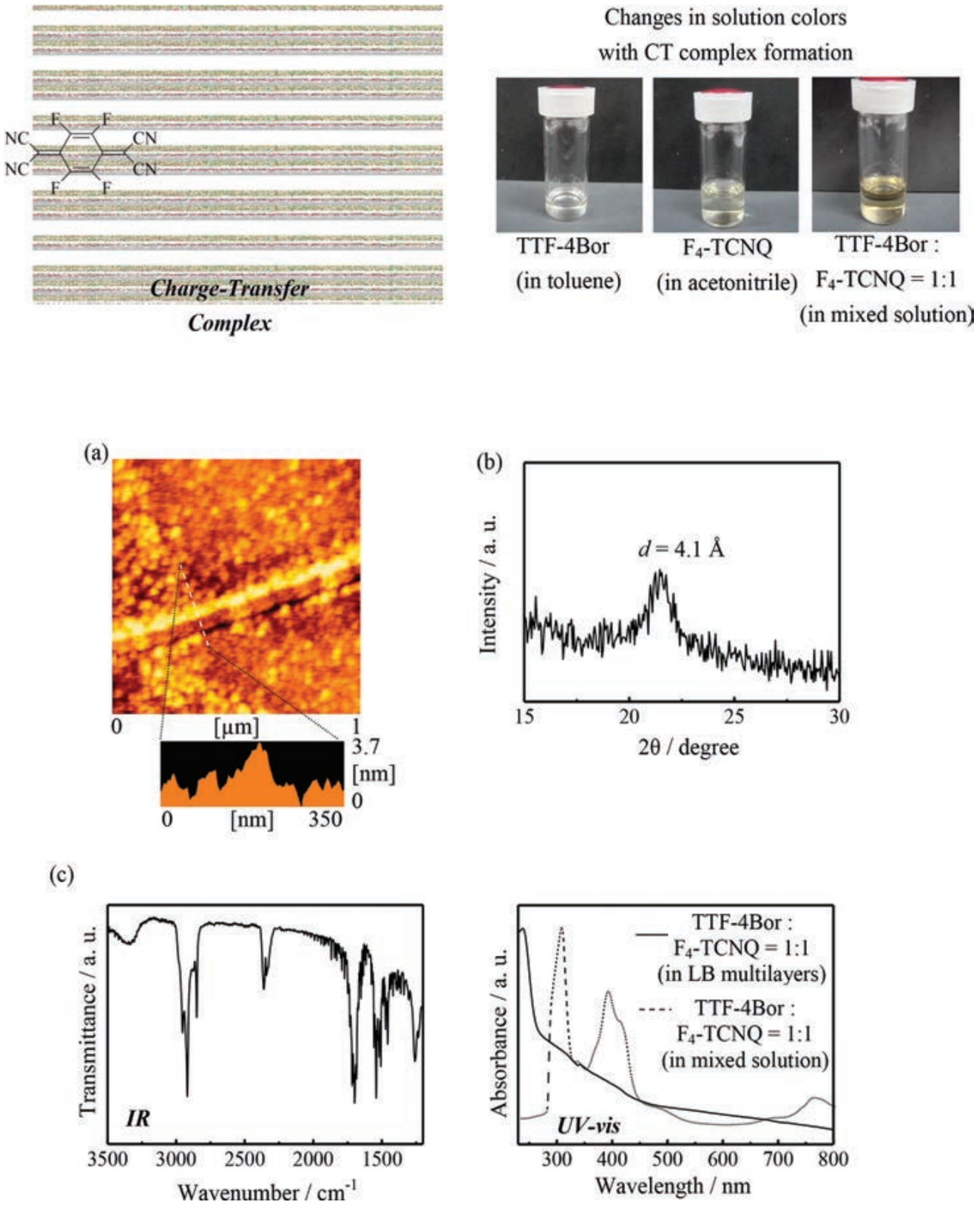

Figure 10. (a) AFM image of Z-type monolayer, (b) in-plane XRD, and (c) IR and UV–Vis spectra of the LB multilayers (20 layers) of TTF derivative/F_4-TCNQ = 1:1 charge transfer complex.

http://dx.doi.org/10.5772/63701

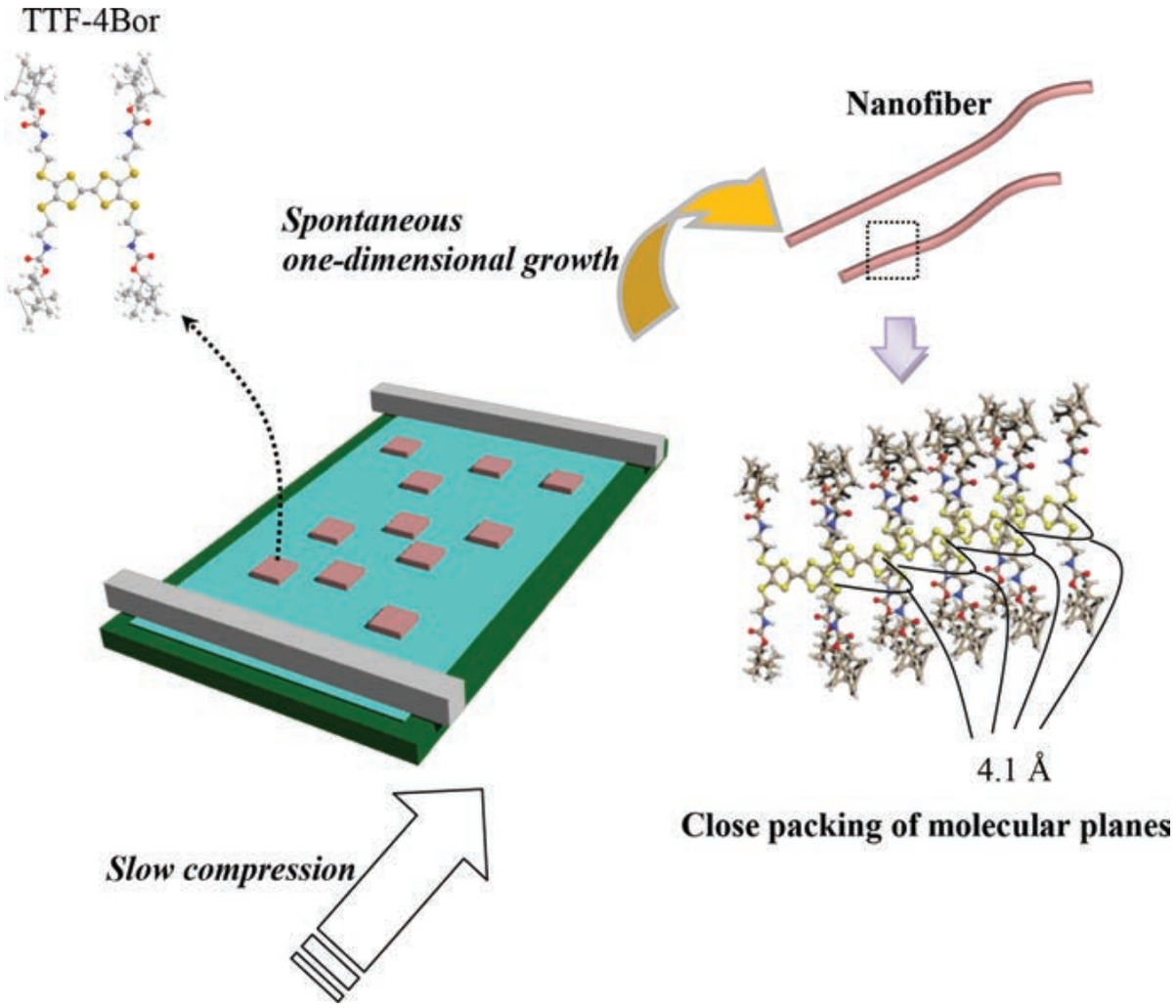

Figure 11. Schematic models for the formation of spiral morphology at the mesoscopic scale, and molecular level stacking of TTF-4Bor by the one-dimensional growth method.

1.4. Conclusions

In this chapter, monolayer behavior on the surface of water, mesoscopic morphological formation, and molecular arrangement in LB multilayers of the conductive TTF derivative with chiral groups were investigated. For this purpose, π–A isotherms, in-plane and out-of-plane XRD, and AFM measurements were carried out. From the AFM analysis, the formation of submicron networks and nanofiber morphology of the conducting molecular organization was confirmed at different monolayer compression rates. The in-plane and out-of-plane XRD measurements elucidated the formation of highly ordered layered structures and close-stacking of molecular planes due to π–π interactions.

Nanofibers of the TTF derivative were obtained by applying the one-dimensional growth method at low compression speeds and low surface pressure conditions. Under these conditions, the formation of helical nanofibers was also observed. These mesoscopic helical nanofibers, whose internal structure consists of stacked conducting planes, are expected to display

spontaneous electrical conduction by electromagnetic induction. Hence, these materials are likely candidates for future innovation in the molecular device and healthcare industries.

2. Morphological control of crystalline nanofiber derived from amphiphilic diamide derivative which induces the thixotropic ability

2.1. Introduction

In the molecular and materials chemistry, the concept of "hierarchy [43]" is very important. In usual, the molecular level orientation and arrangements beyond the level of mesoscopic morphogenesis cannot affect the level of the macroscopic physical properties. However, there are cases that molecular groups with crystalline array achieved a fibrous growth by the cooperative phenomenon of molecules, and its network form occurs thixotropic ability [43]. If this crystalline fiber network contacts to other medium and induces the increase of that viscosity, the corresponding molecule is acting as a thixotropic agent beyond the size hierarchy of materials.

In addition, current nanotechnology in the chemistry and biophysics fields has undergone a remarkable development through the "discovery of the nanosized architecture" such as carbon nanotubes [44], "their deployment to the nanocomposite materials [45–48]", and "re-attention to the bottom-up technologies as the classical LB method [1]". Performance enhancement of analytical techniques, such as scanning probe microscopy and X-ray diffraction, has also helped strongly to the development of nanoscience.

By the way, the thixotropic phenomenon, which solidification and the flow are, respectively, occurred by standing and application of an external forces, is observed in familiar mayonnaise, ketchup, etc. Commercially available anti-sedimentation agent and liquid dripping inhibitors are also used as thixotropic agents. In addition, an additive which can be solidified the cooking waste oil and discarded it as a solid is also corresponding to a thixotropic agent. Traditionally, the main raw material of the thixotropic agent was 12-hydroxystearic acid. In this case, an occurrence origin of thixotropic properties is the fiber growth by 12-hydroxystearic acid molecule at micrometer level. The increase in viscosity has occurred by the contact of this developed microfiber to the corresponding medium. In other words, relationship between fiber growth and occurrence of thixotropic properties is almost equal. However, although the 12-hydroxy stearic acid can form a fibrous morphology in the view of molecular science, stearic acid does not form a fibrous form. It is well-known that stearic acid is the standard material of monolayer on the water surface, and corresponding LB film. Although stearic acid is a crystalline compound, its mesoscopic form is a sheet-like morphology. In other words, the influence of the hydrogen bonding between hydroxyl groups at the 12-position to the formation of the fibrous morphology is remarkable. However, the hydrogen bonding itself is also interaction at the molecular level. It cannot be asserted to affect the mesoscopic morphogenesis and macroscopic thixotropic by only the presence of a simple hydrogen bonding. However, hydrogen bonding "between biological polymers that forms the human body" and "between

http://dx.doi.org/10.5772/63701

the polyamide fibers which is raw materials of a garment," reality induces the macroscopic physical properties. In order to attain an understanding of these phenomena, the material evaluation by the hierarchical point of view will be essential by making full use of nanotechnological analysis developed in recent years. In addition, discussion ability that be considered in connecting these phenomena will be extremely important. However, discussion to the 12-hydroxystearic acid itself has already been a thing of the past on the development of academic field of modern chemistry.

In the present chapter, amphiphilic diamide derivative which obtained by condensation reaction of 12-hydroxystearic acids and hexamethylenediamine was synthesized. The monolayer behavior, molecular arrangement, and surface morphology of organized molecular films of diamide derivative with two hydrocarbons were investigated by analysis of the π–A isotherms, in-plane and out-of-plane XRD profiles, and AFM images. Further, morphogenesis was encouraged by applying the epitaxial growth to a spin-cast film of diamide derivative. The form of the nanofibers thus obtained was indicated the linearly developed shape. Since the internal structure of the mesoscopic nanofiber is comprised of packed hydrocarbons at a molecular level, effective molecular packing is expected along the fiber growing direction.

2.2. Experimental section

2.2.1. Synthesis and characterization of amphiphilic diamide derivative with two hydrocarbons

In order to obtain the material used in this chapter, a condensation reaction of 12-hydroxystearic acid and hexamethylenediamine (2 mol: 1 mol) was performed. The obtained material was purified by recrystallization, and a removal of impurity checked by thermal analysis. **Figure 12(a)** shows thermogravimetric (TG) curves of this material under the N_2 purge and in the air atmosphere. Under the N_2 purge and in the air atmosphere, the decreasing of weight of material is started at 250 and 350°C, respectively. Further, there is a residual of heated material until 500°C and in the air atmosphere. That is to say, this material decomposes like a certain polymer at 250°C and do not sublimate as substance with low molecular weight. In other words, it finds that this compound is an extreme high heat resistance by the influence of hydrogen bonding. **Figure 12(b)** shows differential scanning calorimetric (DSC) thermogram of diamide derivative with two hydrocarbons. Only one transition peaks in both heating and cooling processes exist at around 150 and 135°C, respectively. In the case of unpurified sample, transition peaks of reacted substances in heating process are indicated at around 77 and 42°C. Therefore, it was considered that unreacted 12-hydroxystearic acid and hexamethylenediamine have been removed by recrystallization purification.

2.2.2. Characterization of bulk and their spin-cast film

The spin-cast films of diamide derivative with two hydrocarbons and the mixture with organo-modified layered silicate were formed from xylene– ethanol (9/1, v/v) mixed solution over 100°C. Organo-modified montmorillonite (MMT) was fabricated by surface modification method with natural MMT and long-chain quaternary ammonium cation at oil/water interface [49]. Powder X-ray diffraction (XRD) measurement to the both bulk and cast film samples is

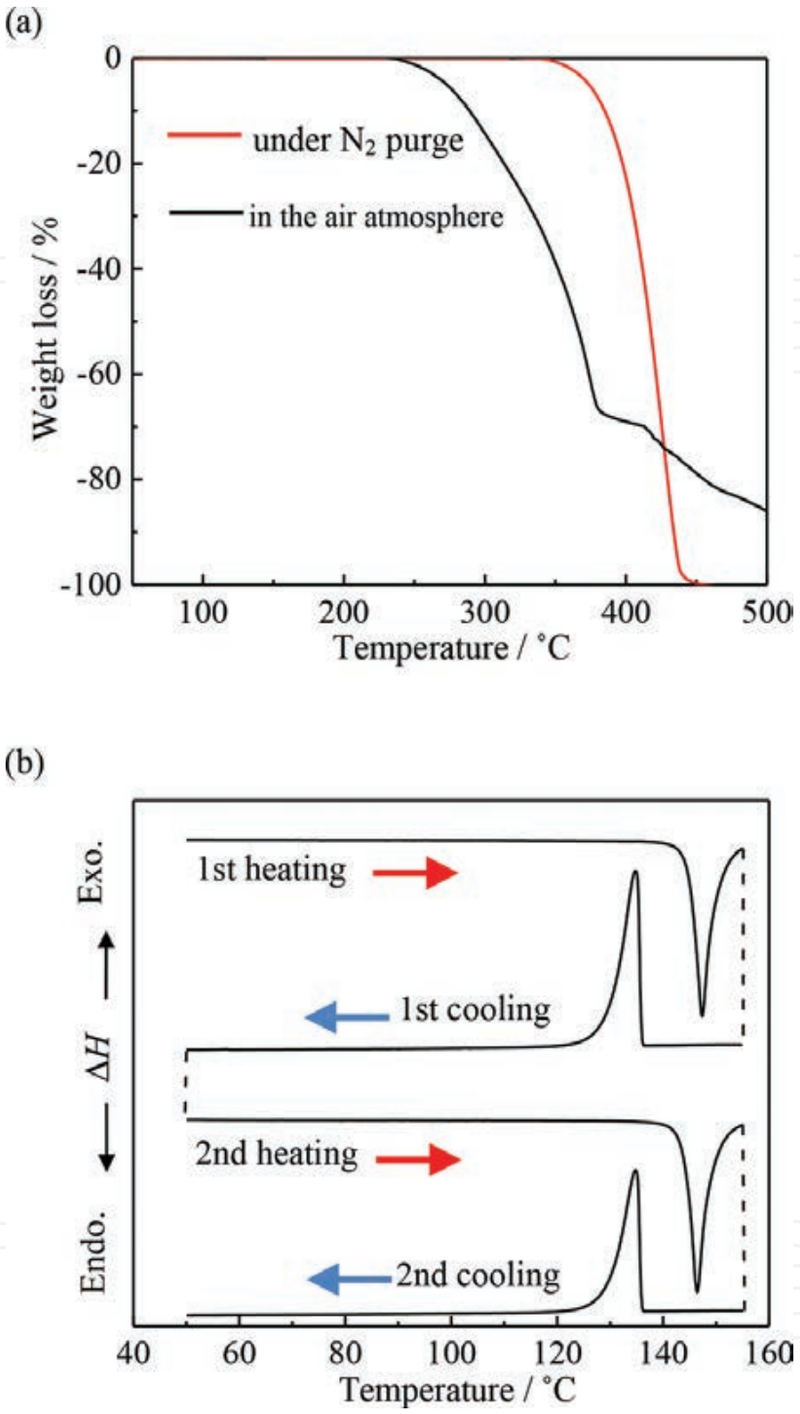

Figure 12. (a) TG curves of diamide derivatives having two hydrocarbons used in this study under the N_2 purge and in the air atmosphere. (b) DSC thermogram of purified diamide derivatives having two hydrocarbons (scanning rate; 10°C min^{-1}).

performed by X-ray diffractometer (Rigaku, Rint-Ultima III, CuKα radiation, 40 kV, 30 mA) equipped with a graphite monochromator. Infrared (IR) spectra of the sample are measured by IR spectrometer (Bruker AXS TENSOR II).

http://dx.doi.org/10.5772/63701

2.2.3. Formation of monolayers of diamide derivative with two hydrocarbons on the water surface

Monolayers were formed by spreading from a $CHCl_3$ solution including a small amount of trifluoroacetic acid (TFA) of diamide derivate having two-stearic chains with –OH groups ($\sim 1.0 \times 10^{-4}$ M) on the surface of distilled water (resistivity: approximately 18.2 MΩ cm). After evaporation of the $CHCl_3$ for 5 min, surface pressure-area (π–A) isotherms were recorded at compression speeds ranging from 4.8 $cm^2\ min^{-1}$. The air/water interface was kept at a constant temperature of 3.5, 12, and 15°C by circulation of thermostated water around the trough. Measurement of the monolayer properties and LB film transfer were carried out in a USI-3-22 Teflon-coated LB trough (USI Instruments). Further, mixed monolayers on the aqueous buffer solution including Na^+ ion of diamide derivative and organo-MMT have been formed by co-spreading method of $CHCl_3$ solution with small amount of TFA and toluene solution, respectively.

2.2.4. Study of the surface morphology and estimation of the molecular arrangement

The surface morphologies of the transferred films were observed using a scanning probe microscope (Atomic Force Microscopy, SII Nanotechnology, SPA300 with SPI-3800 probe station), and microfabricated rectangular Si cantilevers with integrated pyramidal tips, by applying a constant force of 1.4 N m^{-1}. In this chapter, AFM observations were carried out in the tapping mode. XRD samples were transferred onto a glass substrate by the LB method (20 layers, subphase temperature of 15°C, and surface pressures of 35 mN m^{-1}). The large spacing between the layers in the films was measured using an out-of-plane X-ray diffractometer (Rigaku, Rint-Ultima III, CuKα radiation, 40 kV, 30 mA) equipped with a graphite monochromator. The in-plane spacing of the two-dimensional lattice of the films was determined using an X-ray diffractometer with different geometrical arrangements [31, 32] (Bruker AXS, MXP-BX, CuKα radiation, 40 kV, 40 mA, a customized instrument) and equipped with a parabolic graded multilayer mirror. The X-rays were incident at an angle of 0.2°, and the films were scanned at a speed of 0.05°/20 s, as a result of which the in-plane XRD measurements had monomolecular resolution.

2.3. Results and discussion

2.3.1. Molecular arrangement and packing of diamide derivative including two-stearic chains with –OH groups

Figures 13(a) and **(b)** shows the powder XRD profiles and IR spectrum of diamide derivative with two hydrocarbons in bulk. In powder XRD profile, the developed layer spacing is indicated in low angle side. In this case, the long spacing peaks until fifth-order reflection are clearly confirmed. Furthermore, bands of stretching vibration of N–H and O–H are shifted to relative low angle side in IR spectra by the influence on the hydrogen bonding. In addition, amide I and II bands are clearly confirmed at around 1640 and 1550 cm^{-1}.

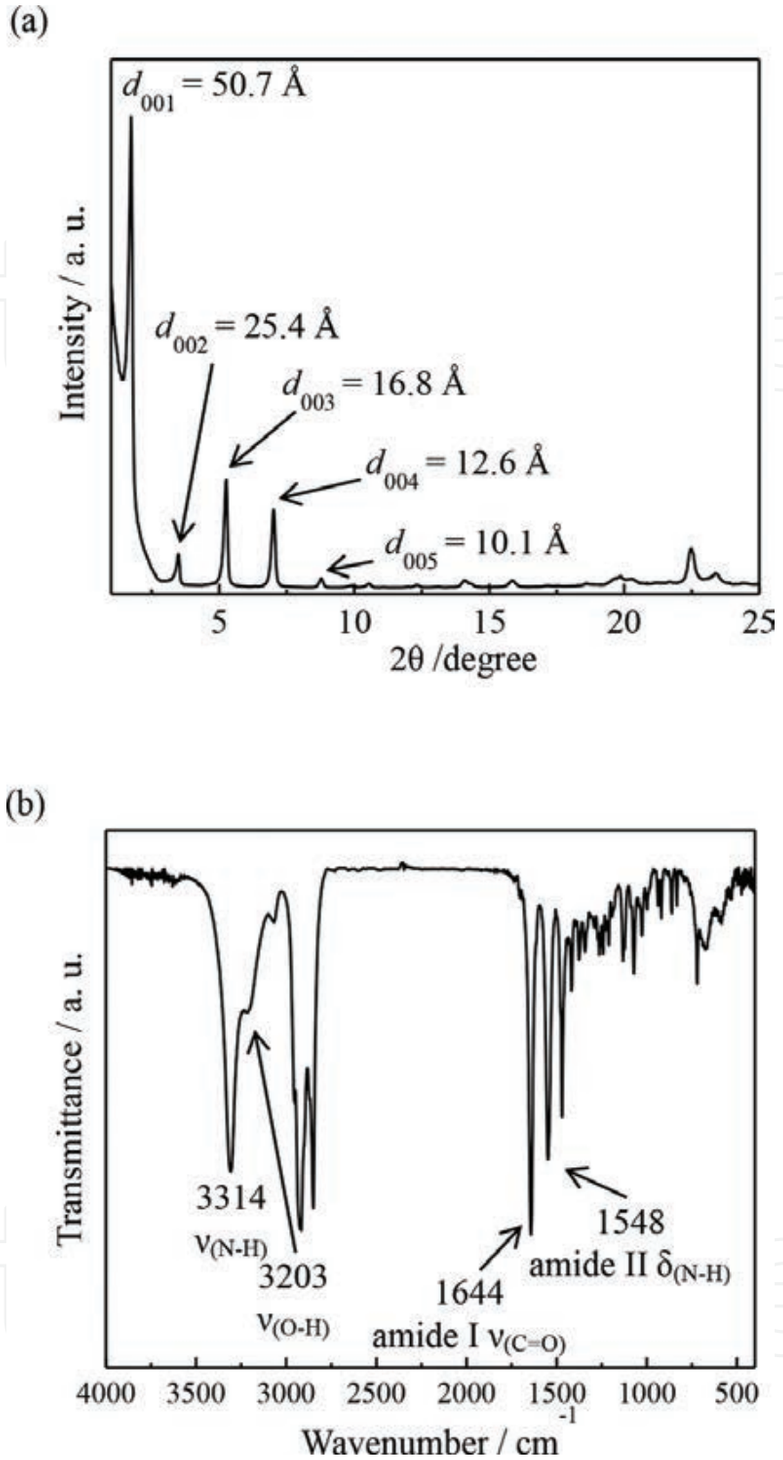

Figure 13. (a) Powder X-ray diffraction profile of diamide derivatives having two hydrocarbons in bulk. (b) IR spectra of diamide derivatives having two hydrocarbons in bulk.

Figure 14 shows the schematic illustration of two kind of possibility of molecular arrangement of diamide derivative with two hydrocarbons in bulk. In the case of model in **Figure 14(a)**, molecules form the extended chain conformation. On the other hand, bilayer structure is formed like a general surfactant molecules in **Figure 14(b)**. In both case, it finds that intermo-

http://dx.doi.org/10.5772/63701

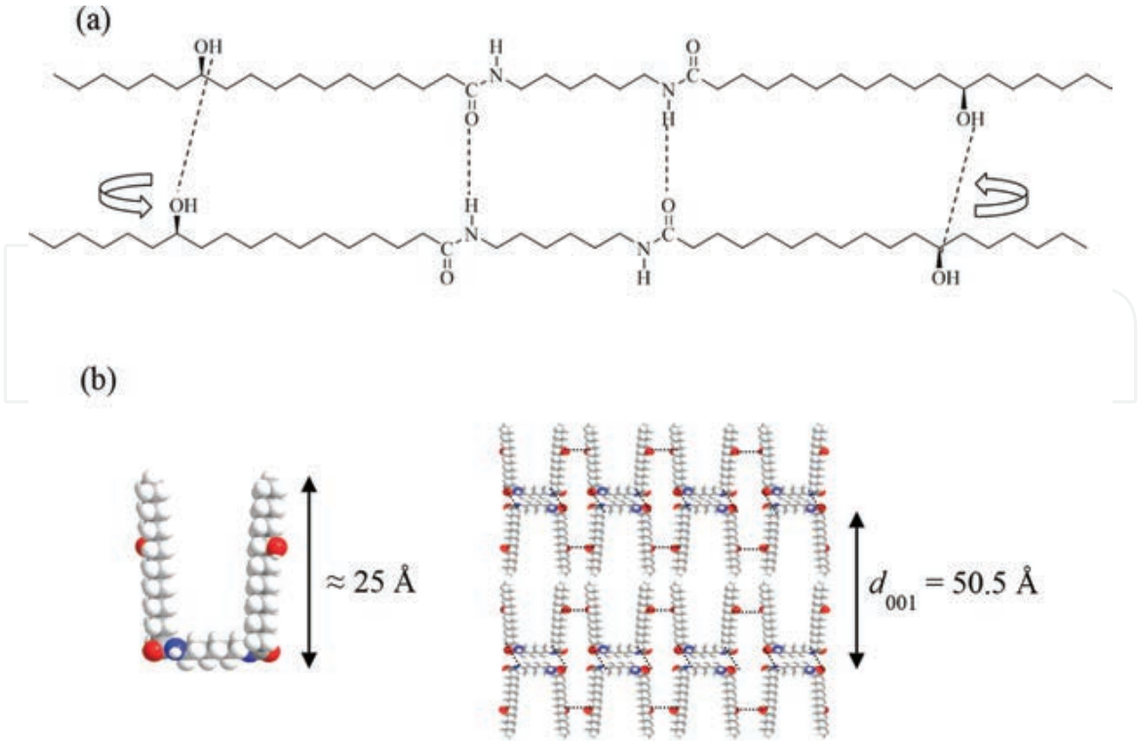

Figure 14. Schematic illustration of two kind of possibility of molecular arrangement of diamide derivatives having two hydrocarbons in bulk. (a) An extended chain model. (b) Double layered structure model.

lecular hydrogen bonding between hydroxyl groups and amide groups have formed by the results of IR. There are two kinds of possibility of molecular orientation that first-order reflection corresponds to tilted single-layer spacing or bilayer spacing. In this stage, both possibilities cannot be rejected. However, authors support bilayer conformation as **Figure 14(b)** according to the nature of this type of amphiphilic materials.

2.3.2. Monolayer behavior and surface morphology of diamide derivative with two hydrocarbons

Figure 15 shows the π–A isotherms of monolayer on the water surface of a diamide derivative with two hydrocarbons at 3.5, 12, and 15°C. At 15°C, isotherm of diamide derivative with two hydrocarbons indicates the overshoot shoulder and plateau region near the 10 mN m^{-1}. On the other hand, the number of two-dimensional phase transition increases in isotherms below 12°C. The origin of these two-dimensional phase transition can be inferred by the AFM measurement to monolayers which are transferred on the solid substrate. **Figure 16** shows the AFM images of LB monolayers of diamide derivative with two hydrocarbons (Z-type) on mica, transferred at 7, 10 and 35 mN m^{-1}. At low surface pressures region after first transition, continuously dotted nanodomains are observed. Next, thin fibrous morphology is confirmed after the second transition. Finally, in the high pressure regions, the developed fiber is formed as their monolayer feature. Therefore, it finds that an each two-dimensional transitions are corresponds to morphological changes of monolayer of diamide derivative with two hydrocarbons.

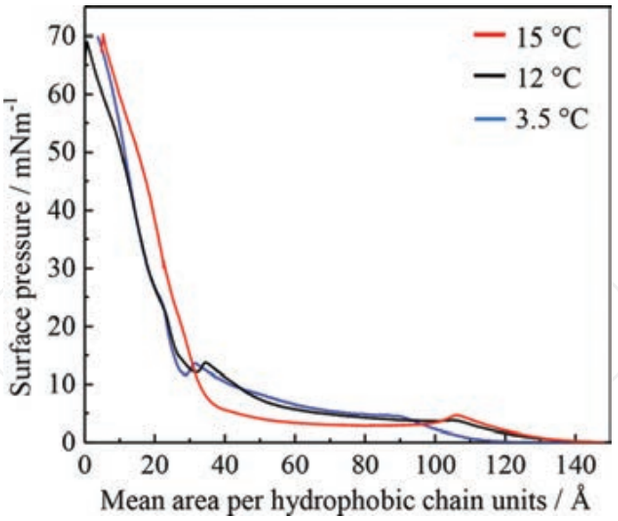

Figure 15. Surface pressure–area isotherms of monolayer on the water surface of diamide derivatives having two-hydrocarbons at 3.5, 12, and 15°C subphase temperature.

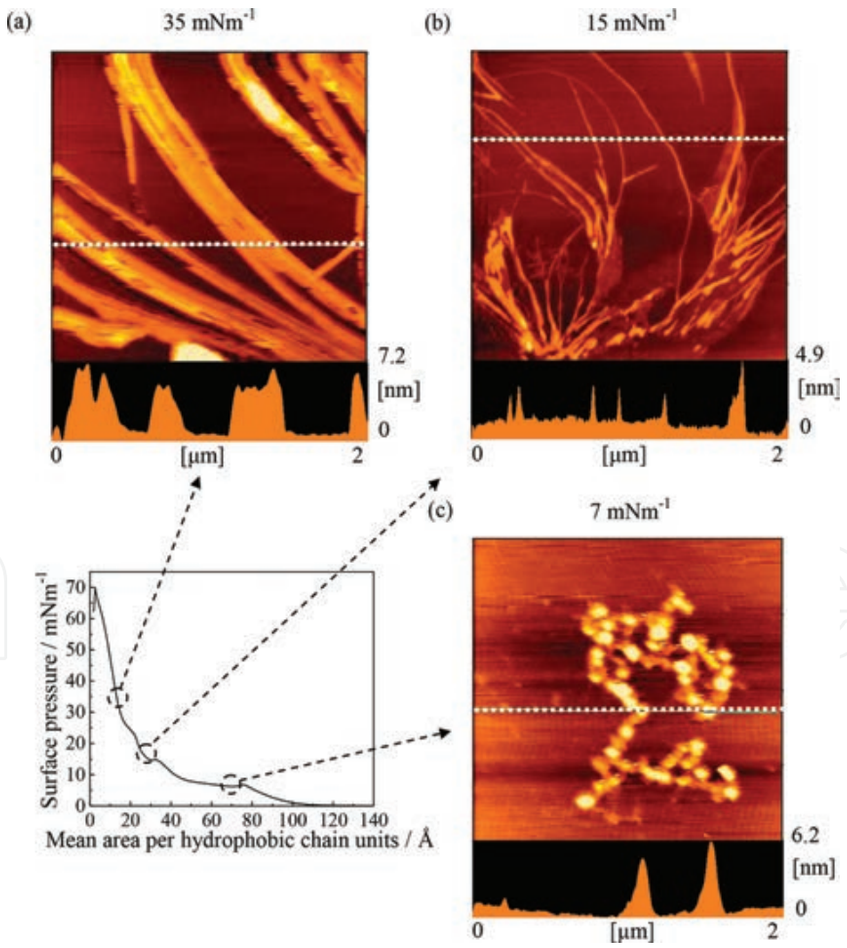

Figure 16. AFM images of monolayer on solid substrate of two-chain-type diamide derivatives transferred at (a) 35 mN m^{-1}, (b) 15 mN m^{-1}, and (c) 7 mN m^{-1} with corresponding isotherm at 12°C.

http://dx.doi.org/10.5772/63701

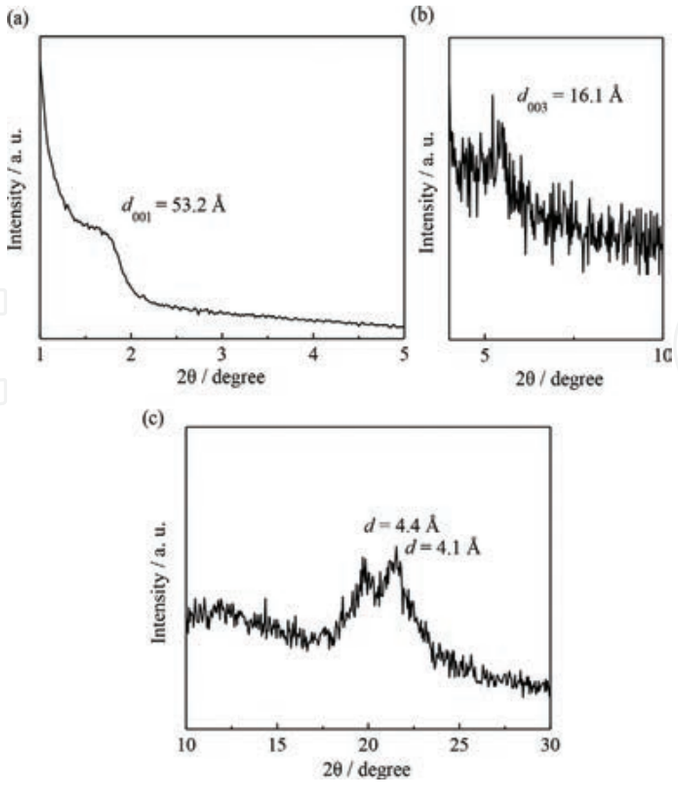

Figure 17. (a, b) Out-of-plane and (c) in-plane XRD profiles of LB multilayers of two-chain-type diamide derivatives transferred at 35 mN m^{-1} and 12°C.

2.3.3. Molecular arrangement in organized molecular films of diamide derivative having two hydrocarbons

In order to estimate the crystallinity and periodicity of the molecules in multilayers of diamide derivative having two hydrocarbons, out-of-plane and in-plane XRD analyses of LB multilayers were carried out. **Figures 17(a)** and **(b)** shows the out-of-plane XRD profiles for LB multilayers (20 layers) which are transferred at 35 mN m^{-1}. In the multilayers fabricated under high surface pressure conditions, it seems that a layer spacing along the *c*-axis at d_{001} = 53.2 Å is corresponding to the bilayer spacing. The shape of first-order reflection is unclear by the influence on the direct beam. However, third-order reflection has also been confirmed. It is expected that highly order layer structure has formed. In-plane XRD profiles of multilayers transferred at 35 mN m^{1} are shown in **Figure 17(c)**. This technique provides information regarding molecular arrangement at a sub-nanometer scale, and the internal fine structure of the mesoscopic fiber morphology. In the LB multilayers formed at crystalline phase, a clear periodic structure with regular molecular packing was confirmed. The short spacing values of 4.4 and 4.1 Å appear to correspond to the packing of the long hydrocarbon chains based on van der Waals interactions. A similar in-plane packing system based on van der Waals interactions between chains, established by in-plane XRD, was reported in organized molecular films of long-chain fatty acid [31]. The packing of hydrocarbons are assigned to two-dimensional orthorhombic system. These results are summarized in **Figure 18**. Due to the nature of the wide angle X-ray diffraction, the exact value of the first-order period (bilayer

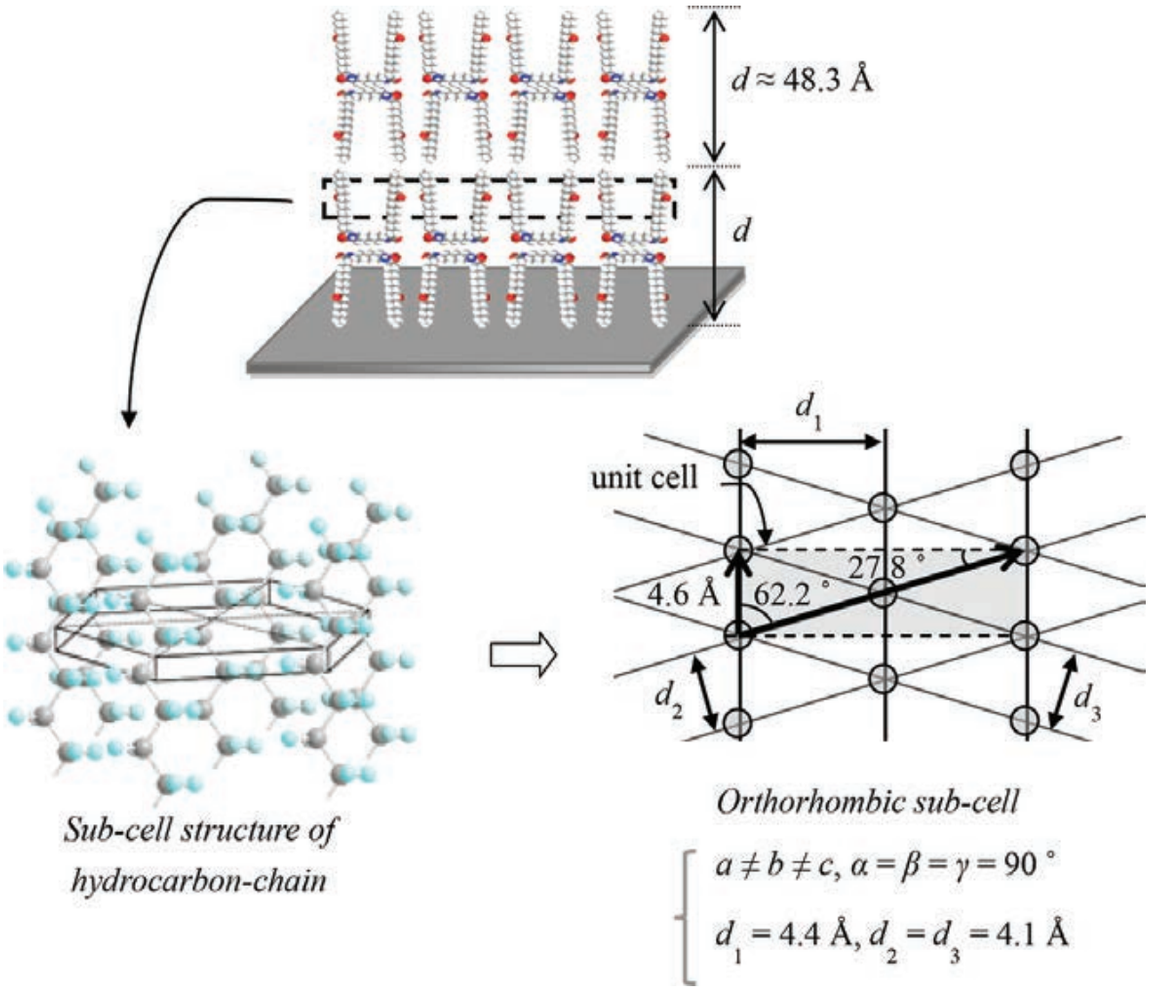

Figure 18. Schematic models of layer structure and sub-cell of hydrocarbons in LB multilayers of two-chain-type diamide derivatives.

spacing) corresponds to three times of $d_{0\,0\,3}$ value (48.3 Å) calculated from the third-order reflection, rather than $d_{0\,0\,1}$ value calculated from the first-order reflection. It finds that formation of the developed layer structure and sub-cell is the feature of this crystalline LB film. Further, bilayer conformation in this LB film is similar to the expected model of this molecule in the bulk state.

2.3.4. Liner morphological growth of nanofibers in a spin-cast film of diamide derivative having two hydrocarbons from layered silicate

At present, there are limitations in the ability to achieve one-dimensional growth of a nanofiber consisting of tightly packed molecules. Although the packed molecules are obtained in the two-dimensional interfacial film at high surface pressures, morphologies at the mesoscopic scale are too entangled and undulated due to the strong forces of aggregation, with the presence of long-range order between molecules, as a result of the competitive effect of van der Waals interactions and hydrogen bonding. Hence, if formation of the packed molecular arrangement is accelerated by the external forces at molecular level, the mesoscopic fiber

http://dx.doi.org/10.5772/63701

growth might be linearly and hierarchically developed. In this chapter, the technique of epitaxial growth from harmless layered material in the mesoscopic spin-cast film was adopted, which used general organic solvent with relative low harmful effect at high temperature, inducing a spontaneous growth structure at the interface. **Figure 19(a)** and **(b)** shows AFM images of spin-cast film of diamide derivative and their composite with 1 wt% organo-modified MMT, respectively. From the comparison between these figures, it is confirmed that essential entanglement and wavy fibers have been performed the one-dimensional growth and changed to the linear shape in the spin-cast film by organo-MMT addition. As shown the results of XRD of **Figure 20** in the Supporting Information, a organo-MMT is also the developed layer-organization with 38 Å double-layered period [50]. Here, it will consider the interaction between organo-modified MMT and two-chain-type diamide derivative.

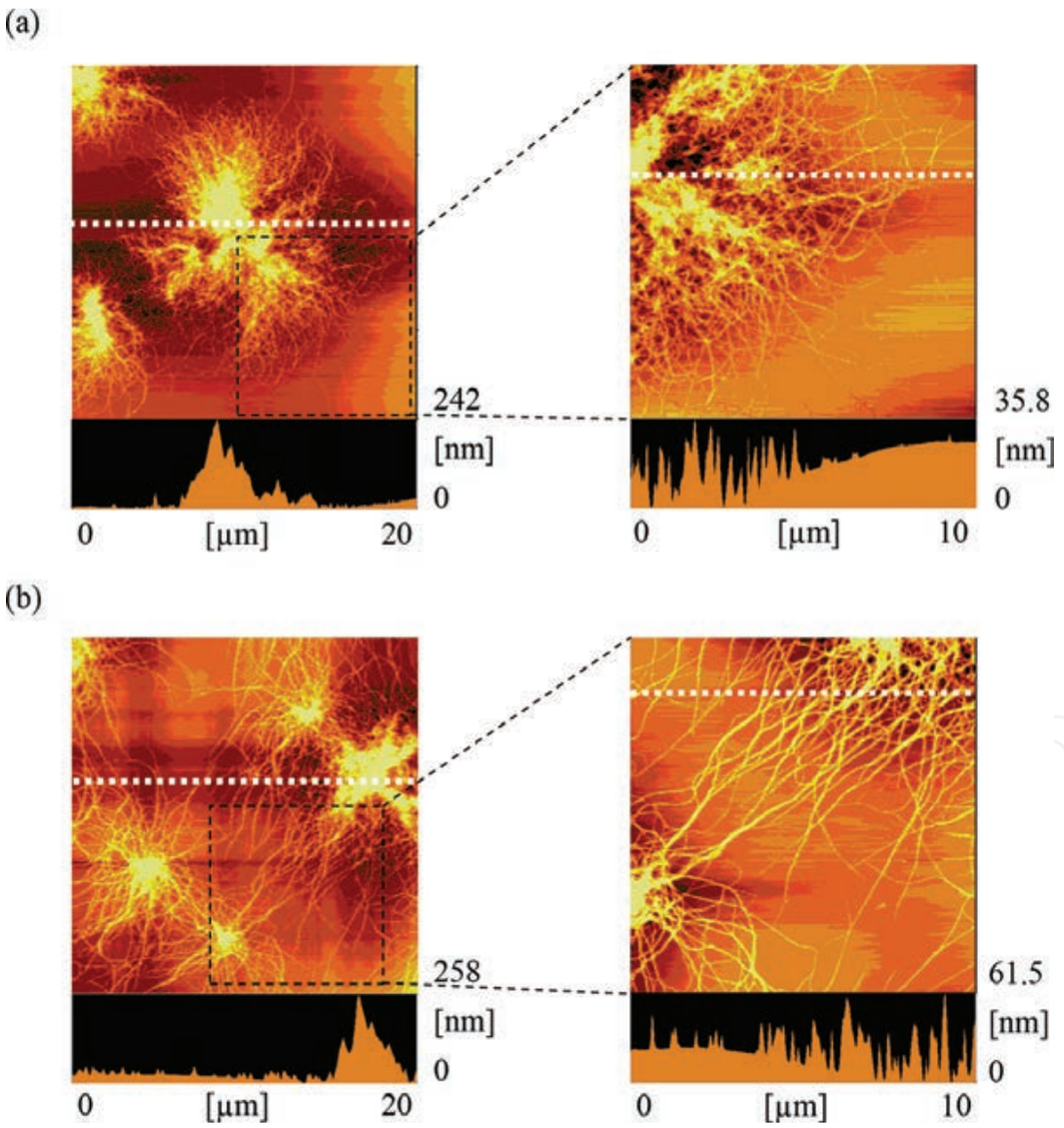

Figure 19. AFM images of spin-cast films of (a) neat diamide derivatives having two hydrocarbons and (b) their composite with 1 wt% organo-modified MMT.

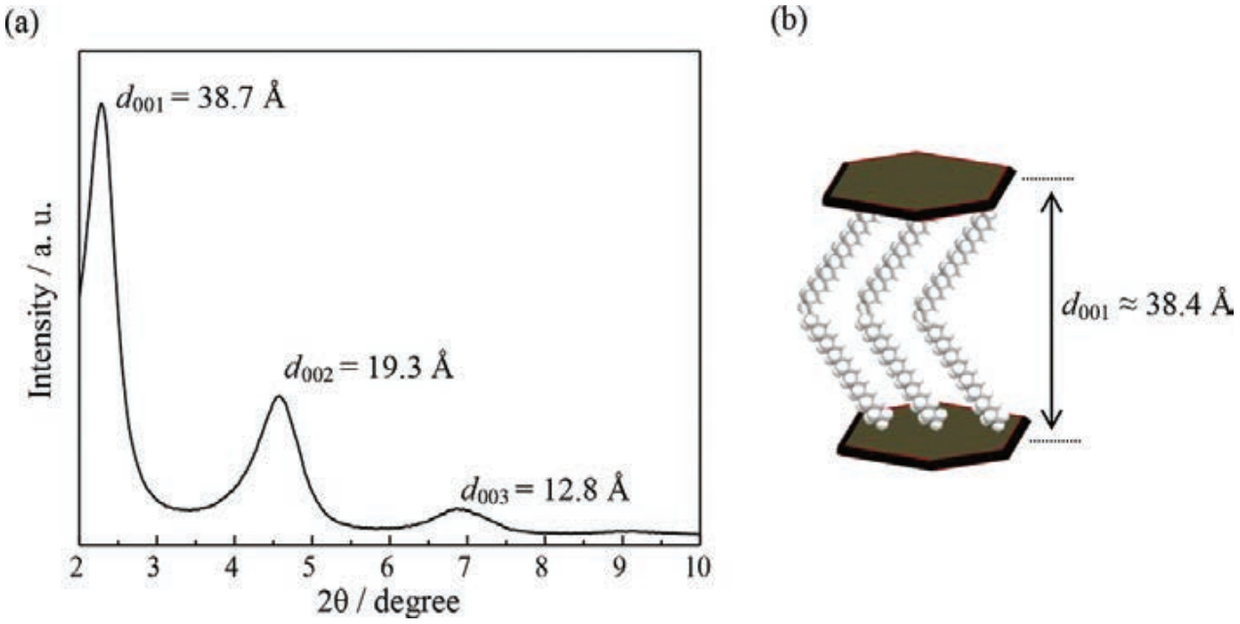

Figure 20. (a) Powder X-ray diffraction profile of organo-modified MMT used in this study [50]. (b) Schematic illustration of layer structure of organo-modified MMT in bulk.

Figure 21(a) indicates the π–A isotherms of the mixed monolayer of two-chain-type diamide derivative: organo-modified MMT = 3:1 and 1:1. Compared to behavior of an each original monolayers, since a change in the collapsed surface pressure occurs, it can be understood the existence of interaction between components. In AFM observation to this mixed monolayer transferred on solid substrate, the fibers of diamide derivative are in contact with the organo-MMT without phase separation, which can be understood to be a system of an ideal mixing (**Figure 21(b)**). Next, the results of XRD of spin-cast films of **Figure 19** are shown (**Figure 22(a)**). (Here, since the presence of the organo-MMT is a very small amount, they are not observed as the IR signal and this spectrum indicates very similar features to that in bulk as shown the IR result of **Figure 23** in the Supporting Information.) From the comparison between both profiles, it finds that the third-order reflection has appeared and the intensity of the second-order reflection slightly decreased by organo-MMT addition. Considering from the concept of odd–even effect of high-order reflection, it seems that "an expression of the higher-order reflection" and "the occurrence of odd–even tendency" indicate an enhancement of regularity (**Figure 22(b)**). As the supporting of this speculation, the intensity of out-of-plane XRD profile of diamide derivative–organo-clay = 1:1 mixed multilayers clearly is increased to the one of the film of single diamide derivative, which is based on the enhancement of regularity along the *c*-axis by addition of organo-clay (**Figure 22(c)**). A schematic diagram which summarizes the above discussion has shown in **Figure 24**. That is to say, it is found that the epitaxial growth along the (0 0 *l*) plane based on the similar long-spacing value of about 4 nm is induced from the affinity of diamide derivative and the long-alkyl chain on the montmorillonite surface.

http://dx.doi.org/10.5772/63701

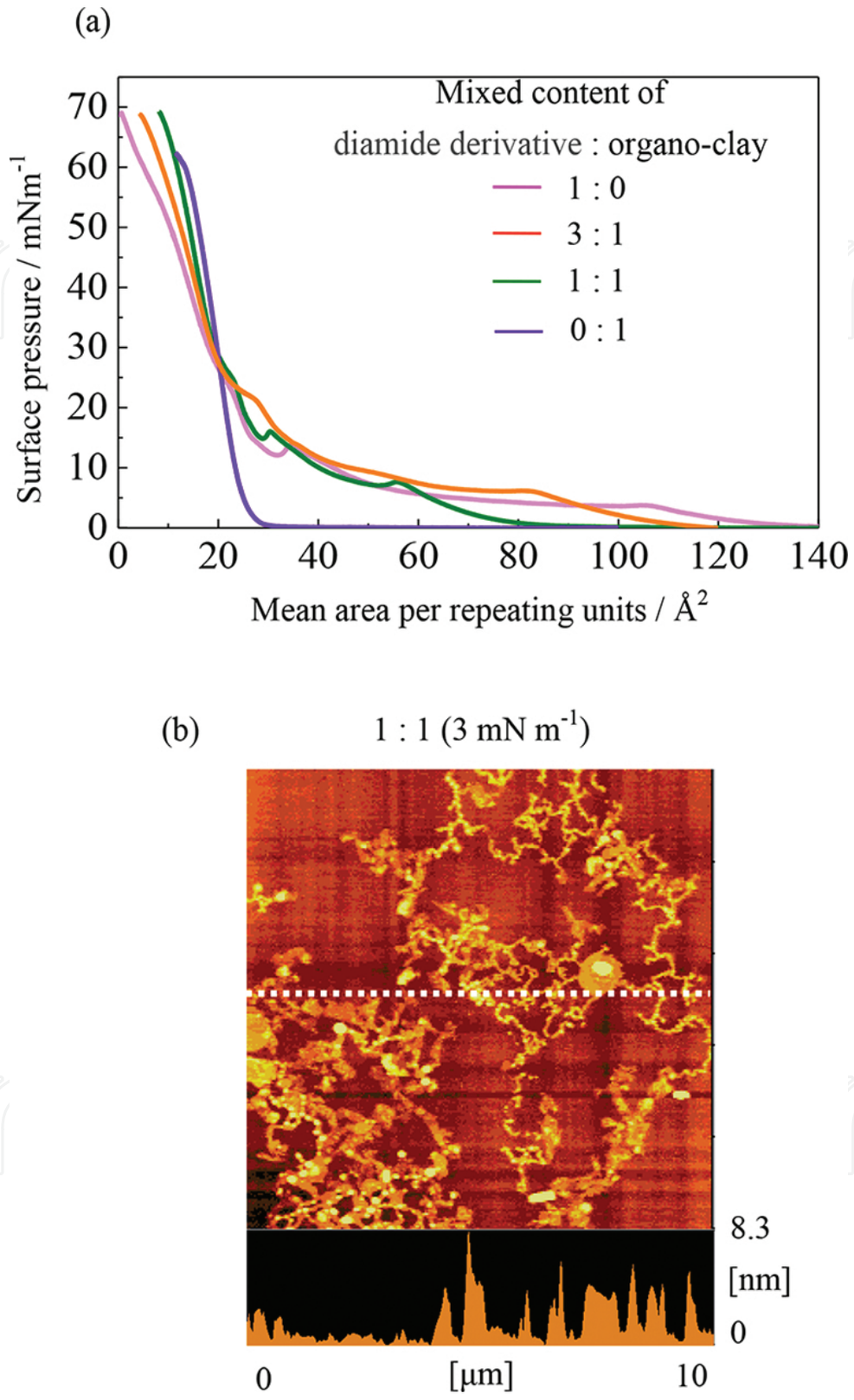

Figure 21. (a) Surface pressure–area isotherms of mixed monolayer on an aqueous buffer solution with Na^+ ion of diamide derivatives having two hydrocarbons:organo-MMT = 1:1 at 12°C. (b) AFM image of Z-type mixed monolayer on solid of diamide derivatives having two hydrocarbons–organo-MMT = 1:1 transferred at 3 mN m^{-1}.

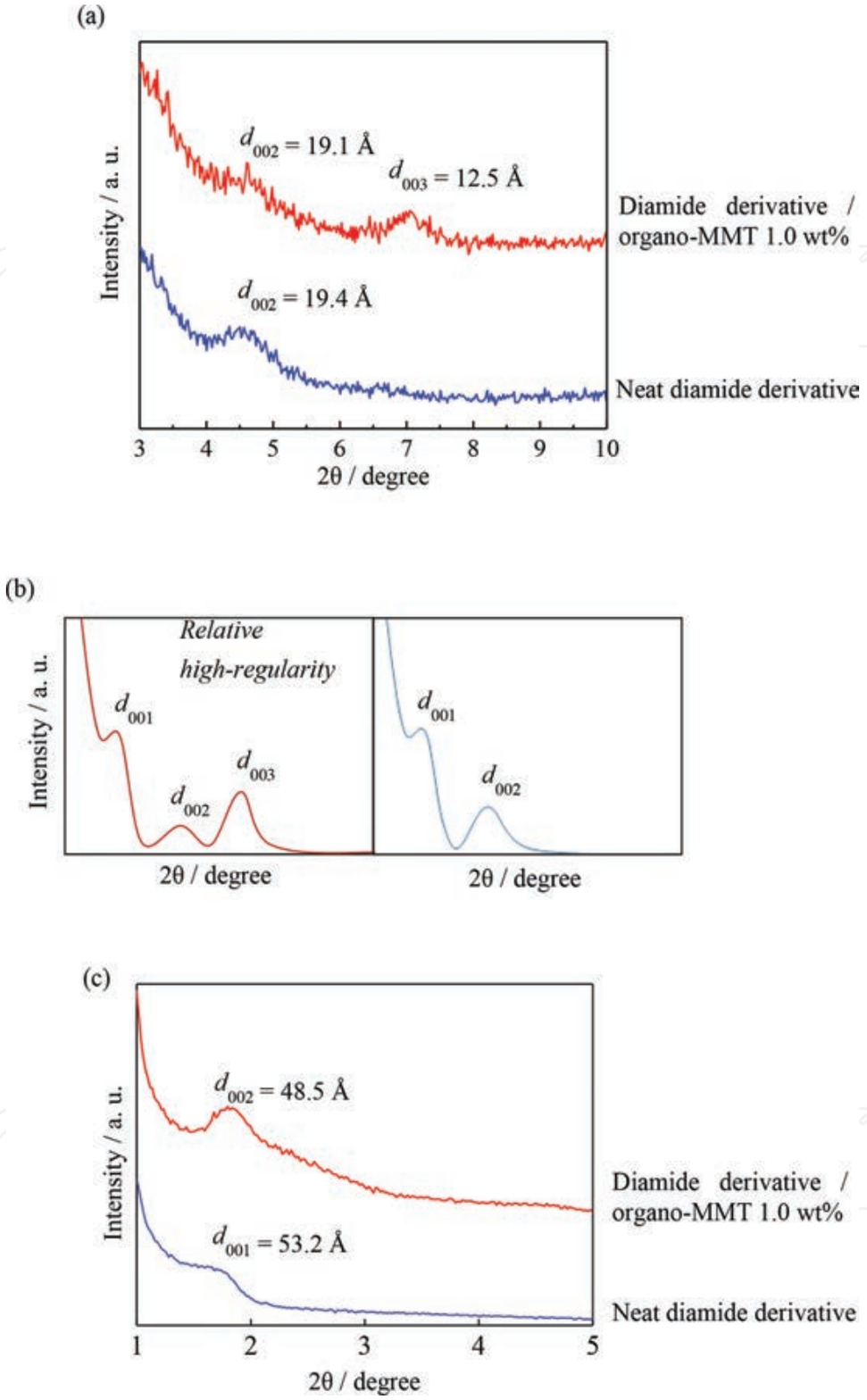

Figure 22. (a) XRD profiles of spin-cast films of neat diamide derivatives having two hydrocarbons and their composite with 1 wt% organo-modified MMT. (b) Simulation of XRD profiles of the layered materials influenced by an odd–even effect. (c) Out-of-plane XRD profiles of LB multilayers of neat diamide derivatives having two hydrocarbons and 1:1 mixed monolayer with organo-modified MMT.

http://dx.doi.org/10.5772/63701

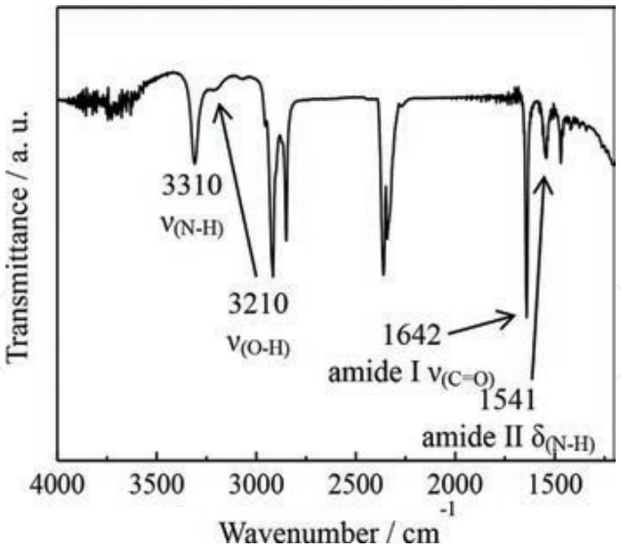

Figure 23. IR spectrum of mixed spin-cast film of two-chain-type diamide derivative with 1 wt% organo-modified MMT.

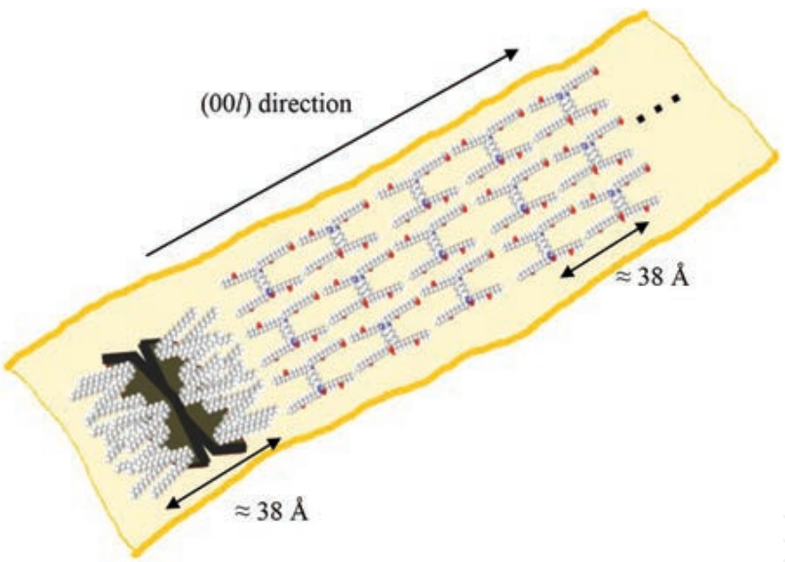

Figure 24. Schematic illustration of epitaxial growth of nanofiber morphology of two-chain-type diamide derivative from organo-modified MMT in spin-cast film.

2.4. Conclusions

In this chapter, monolayer behavior on the water surface, mesoscopic morphological formation, and molecular arrangement in LB multilayers of the diamide derivative having two hydrocarbons were investigated. For this purpose, π–A isotherms, in-plane and out-of-plane XRD, and AFM measurements were carried out. From the AFM analysis, the formation of nanofiber morphology of the thixotropic molecular organization was confirmed at different surface pressures. The in-plane and out-of-plane XRD measurements elucidated the formation

of highly ordered layered structures and close-packing of molecular chains due to van der Waals interaction.

Nanofibers of the two-chain-type diamide derivative were obtained by applying the epitaxial growth method in spin-cast film. Under these conditions, the formation of linearly developed nanofibers was also observed. These mesoscopic extended nanofibers, whose internal structure consists of the packed long-alkyl chain, are expected to display cooperative thixotropic ability by fiber growth. Hence, these materials are likely candidates for future innovation in an additive, waste oil treatment agent, and paint industries.

Acknowledgements

The authors greatly appreciate Mr. Eiichi Sato, Kusumoto Chemicals Ltd., and Dr. Yoko Tatewaki, Tokyo University of Agriculture and Technology for their kind providing of samples. The authors also thank Mr. Kyohei Ohmura and Mr. Takahiro Kikkawa, Saitama University for his kind help of data analysis.

Author details

Manami Iizuka[1], Rie Yamato[2] and Atsuhiro Fujimori[1*]

*Address all correspondence to: fujimori@fms.saitama-u.ac.jp

1 Graduate School of Science and Engineering, Faculty of Engineering, Saitama University, Shimo-Okubo, Saitama, Japan

2 Department of Functional Materials Science, Faculty of Engineering, Saitama University, Shimo-Okubo, Saitama, Japan

References

[1] Blodgett K. Monomolecular Films of Fatty Acids on Glass. J. Am. Chem. Soc. 1934;56: 495–495. doi:10.1021/ja01317a513

[2] Kumaki J, Kawauchi T, Yashima E. Two-Dimensional Folded Chain Crystals of a Synthetic Polymer in a Langmuir–Blodgett Film. J. Am. Chem. Soc. 2005;127:5788–5789. doi:10.1021/ja050457e

[3] Mann B, Kuhn H. Tunneling through Fatty Acid Salt Monolayers. J. Appl. Phys. 1971;42:4398–4405. doi:10.1063/1.1659785

[4] Mann B, Kuhn H, Szentpály Lv. Tunnelling through Fatty Acid Monolayers and its Relevance to Photographic Sensitization. Chem. Phys. Lett. 1971;8:82–84. DOI: 10.1016/0009-2614(71)80582-1

[5] Onouchi H, Okoshi K, Kajitani T, Sakurai S, Nagai K, Kumaki J, Onitsuka K, Yashima E. Two- and Three-Dimensional Smectic Ordering of Single-Handed Helical Polymers. J. Am. Chem. Soc. 2008;130:229–236. doi:10.1021/ja074627u

[6] Kumaki J, Kajitani T, Nagai K, Okoshi K, Yashima E. Visualization of Polymer Chain Conformations in Amorphous Polyisocyanide Langmuir–Blodgett Films by Atomic Force Microscopy. J. Am. Chem. Soc. 2010;132:5604–5606. doi:10.1021/ja908426u

[7] Wu C, Li M, Chi S, Jun G. Laser Light Scattering Characterization of a Novel Polymer Nanofiber. Macromolecules 1998;31:7553–7554. doi:10.1021/ma9800663

[8] Huang MH, Mao S, Feick H, Yan H, Wu Y, Kind H, Weber E, Russo R, Yang P. Room-Temperature Ultraviolet Nanowire Nanolasers. Science 2001;292:1897–1899. doi: 10.1126/science.1060367

[9] Bumm LA, Arnold JJ, Cygan MT, Dunbar TD, Burgin TP, Jones L, Allara DL, Tour JM, Weiss PS. Are Single Molecular Wires Conducting? Science 1996;271:1705–1707. doi: 10.1126/science.271.5256.1705

[10] Fujimori A, Kaneko Y, Kikkawa T, Chiba S, Shibasaki Y. Fabrication and Structure of "Polymer Nanosphere Multilayered Organization". J. Colloid Interf. Sci. 2014;418:338–349. doi:10.1016/j.jcis.2013.12.038

[11] Park K, Sung Y, Han S, Yun Y, Hyeon T. Origin of the Enhanced Catalytic Activity of Carbon Nanocoil-Supported PtRu Alloy Electrocatalysts. J. Phys. Chem. B 2004;108:939–944. doi:10.1021/jp0368031

[12] Liu Y, Li H, Tu D, Ji Z, Wang C, Tang Q, Liu M, Hu W, Liu Y, Zhu D. Controlling the Growth of Single Crystalline Nanoribbons of Copper Tetracyanoquinodimethane for the Fabrication of Devices and Device Arrays. J. Am. Chem. Soc. 2006;128:12917–12922. doi:10.1021/ja0636183

[13] Johnston E, Bullock S, Uilk J, Gatenholm P, Wynne K. Networks from α,ω-Dihydroxypoly(dimethylsiloxane) and (Tridecafluoro-1,1,2,2-tetrahydrooctyl) triethoxysilane: Surface Microstructures and Surface Characterization. Macromolecules 1999;32:8173–8182. doi:10.1021/ma990628y

[14] Masuya R, Ninomiya N, Fujimori A, Nakahara H, Masuko T. Fine Structure and Phase Transition Behavior of Fluorinated Comb Copolymers. J. Polym. Sci. B, Polym. Phys. 2006;44:416–425. doi:10.1002/polb.20711

[15] Klok H, Langenwalter J, Lecommandoux S. Self-Assembly of Peptide-Based Diblock Oligomers. Macromolecules 2000;33:7819–7826. doi:10.1021/ma0009606

[16] Liu F, Prehm M, Zeng X, Tschierske C, Ungar G. Skeletal Cubic, Lamellar, and Ribbon Phases of Bundled Thermotropic Bolapolyphiles. J. Am. Chem. Soc. 2014;136:6846–6849. doi:10.1021/ja502410e

[17] Komiyama H, Sakai R, Hadano S, Asaoka S, Kamata K, Iyoda T, Komura M, Yamada T, Yoshida H. Enormously Wide Range Cylinder Phase of Liquid Crystalline PEO-*b*-PMA(Az) Block Copolymer. Macromolecules 2014;47:1777–1782. doi:10.1021/ma402356z

[18] Yabu H, Jia R, Matsuo Y, Ijiro K, Yamamoto S, Nishino F, Takaki T, Kuwahara M, Shimomura M. Preparation of Highly Oriented Nano-Pit Arrays by Thermal Shrinking of Honeycomb-Patterned Polymer Films. Adv. Mater. 2008;20:4200–4204. doi:10.1002/adma.200801170

[19] Tatewaki Y, Hatanaka T, Tsunashima R, Nakamura T, Kimura, M, Shirai H. Conductive Nanoscopic Fibrous Assemblies Containing Helical Tetrathiafulvalene Stacks. Chem. An Asian J. 2009;4:1474–1479. doi:10.1002/asia.200900044

[20] Tatewaki Y, Watanabe T, Watanabe K, Kikuchi K, Okada S. Synthesis and Nanostructures of Several Tetrathiafulvalene Derivatives Having the Side Chains Composed of Chiral and Hydrogen-Bonding Groups and their Charge-transfer Complexes. Dalton Trans. 2013;42:16121–16127. doi:10.1039/C3DT51464A

[21] Gaines Jr, G. L. Insoluble Monolayers at Liquid Gas Interfaces; Wiley: New York, 1966.

[22] Kuhn H, Möbius D, Bücher H. Spectroscopy of Monolayer Assemblies, In Physical Methods of Chemistry; Weissberger, A.; Rossiter, B. W., Eds.; Wiley: New York, 1972, Vol. 1, Part IIIB, p. 577–702.

[23] (a) Roberts GG. Langmuir–Blodgett Films; Plenum Press: London, 1990. ISBN: 978-1-4899-3716-2; (b) Petty MC. Langmuir–Blodgett Films; Cambridge Univ. Press: New York, 1996. ISBN: 9780521424509

[24] Ulman A. An Introduction to Ultrathin Organic Films: from Langmuir–Blodgett to Self-assembly; Academic Press: Boston, 1991. ISBN : 9780127082301

[25] Fukuda K, Shiozawa T. Conditions for Formation and Structural Characterization of X-type and Y-type Multilayers of Long-chain Esters. Thin Solid Films 1980;68:55–66. doi:10.1016/0040-6090(80)90136-4

[26] Fukuda K, Shiozawa T. Structural Control and Characterization in Mixed and Alternate Langmuir–Blodgett Films of Simple Long-chain Compounds. Thin Solid Films 1989;178:421–425. doi:10.1016/0040-6090(89)90332-5

[27] Fukuda K, Shibasaki Y, Nakahara H. Effects of Molecular Arrangement on Polymerization Reactions in Langmuir–Blodgett Films. Thin Solid Films 1983;99:87–94. doi:10.1016/0040-6090(83)90363-2

[28] Fukuda K, Shibasaki Y, Nakahara H. Molecular Arrangement and Polymerizability of Amino Acid Derivatives and Dienoic Acid in Langmuir–Blodgett Films. Thin Solid Films 1985;133:39–49. doi:10.1016/0040-6090(85)90423-7

[29] Fukuda K, Shibasaki Y, Nakahara H. Polymerizabilities of Amphiphilic Monomers with Controlled Arrangements in Langmuir–Blodgett Films. Thin Solid Films 1988;160:43–52. doi:10.1016/0040-6090(88)90045-4.

[30] Spooner SP, Whitten DG. Photoreactions in Monolayer Films and Langmuir–Blodgett Assemblies, In Photochemistry in Organized & Constrained Media; Ramamurthy, V., Ed.; VCH Pub.: New York, 1991. Chap 15. 691–738 p.

[31] Fujimori A, Sugita Y, Nakahara H, Ito E, Hara M, Matsuie N, Kanai K, Ouchi Y, Seki K. Change of Molecular Packing and Orientation from Monolayer to Multilayers of Hydrogenated and Fluorinated Carboxylates Studied by In-plane X-ray Diffraction together with NEXAFS Spectroscopy at CK-edge. Chem. Phys. Lett. 2004;387:345–348. doi:10.1016/j.cplett.2004.02.032

[32] Fujimori A, Araki T, Nakahara H, Ito E, Hara M, Ishii H, Ouchi Y, Seki K. In-plane X-ray Diffraction and Polarized NEXAFS Spectroscopic Studies on the Organized Molecular Films of Fluorinated Amphiphiles with Vinyl Esters and their Comb-polymers. Chem. Phys. Lett. 2001;349:6–12. doi:10.1016/S0009-2614(01)01196-4

[33] Tatewaki Y, Okada S, Itagaki R, Nakamura T, Fujimori A. Study of Molecular Arrangement of Organized Molecular Films of Charge-Transfer Complexes Containing 1, 3-Dithiole-2-Thione-4, 5-Dithiolate by In-plane and Out-of-plane X-ray Diffractions. J. Colloid Interf. Sci. 2010;343:281–290. doi:10.1016/j.jcis.2009.09.031

[34] Jung JH, Ono Y, Shinkai S. Sol-Gel Polycondensation in a Cyclohexane-Based Organogel System in Helical Silica: Creation of both Right- and Left-Handed Silica Structures by Helical Organogel Fibers. Chem. Eur. J. 2000;6:4552–4557. doi: 10.1002/1521-3765(20001215)6:24<4552::AID-CHEM4552>3.0.CO;2-5;

[35] Jung JH, Ono Y, Shinkai S. Sol-Gel Polycondensation of Tetraethoxysilane in a Cholesterol-Based Organogel Synstem Results in Chiral Spiral Silica. Angew. Chem. Int. Ed. 2000;39:1862–1865. doi:10.1002/(SICI)1521-3773(20000515)39:10<1862::AID-ANIE1862>3.0.CO;2-3;

[36] Jung JH, Kobayashi H, Mitsutoshi M, Shimizu T, Shinkai S. Helical Ribbon Aggregate Composed of a Crown-Appended Cholesterol Derivative Which Acts as an Amphiphilic Gelator of Organic Solvents and as a Template for Chiral Silica Transcription. J. Am. Chem. Soc. 2001;123:8785–8789. doi:10.1021/ja010508h.

[37] Jha SK, Cheon K, Green MM, Selinger JV. Chiral Optical Properties of a Helical Polymer Synthesized from Nearly Racemic Chiral Monomers Highly Diluted with Achiral Monomers. J. Am. Chem. Soc. 1999;121:1665–1673. doi:10.1021/ja983202s

[38] Green MM, Khatri C, Peterson NC. A Macromolecular Conformational Change Driven by a Minute Chiral Solvation Energy. J. Am. Chem. Soc. 1993;115:4941–4942. doi: 10.1021/ja00064a086

[39] Konuma T, Akutagawa T, Yumoto T, Nakamura T, Kawamata J, Inoue K, Nakamura T, Tachibana H, Matsumoto M, Ikegami K, Horiuchi H, Yamochi H, Saito G. Charge-transfer Interactions and Non-linear Optical Properties of Tetrathiafulvalene-based Langmuir–Blodgett Films. Thin Solid Films 1998;327–329:348–352. DOI:10.1016/S0040-6090(98)00667-1

[40] Horiuchi S, Yamochi H, Saito G, Sakaguchi K, Kusunoki M. Nature and Origin of Stable Metallic State in Organic Charge-Transfer Complexes of Bis(ethylenedioxy)tetrathiafulvalene. J. Am. Chem. Soc. 1996;118:8604–8622. doi:10.1021/ja960393v

[41] Torrance JB, Scot BA, Welber B, Kaufman FB, Seiden PE. Optical Properties of the Radical Cation Tetrathiafulvalenium (TTF^+) in its Mixed-valence and Monovalence Halide Salts. Phys. Rev. B: Condens Matter 1979;19:730–741. doi:10.1103/PhysRevB.19.730

[42] Bradshaw D, Claridge JB, Cussen EJ, Prior TJ, Rosseinsky MJ. Design, chirality, and flexibility in nanoporous molecule-based materials. Accounts Chem. Res. 2005;38:273–282. doi:10.1021/ar0401606

[43] Barnes HA. Thixotropy—A review. J. Non-Newtonian Fluid Mech. 1997;70:1–33. doi: 10.1016/S0377-0257(97)00004-9

[44] Karimi-Maleh H, Tahernejad-Javazm F, Ensafi AA, Moradi R, Reza, Mallakpour S, Beitollahi H. A high sensitive biosensor based on FePt/CNTs nanocomposite/N-(4-hydroxyphenyl)-3,5-dinitrobenzamide modified carbon paste electrode for simultaneous determination of glutathione and piroxicam. Biosens. Bioelectron. 2014;60:1–7. doi: 10.1016/j.bios.2014.03.055

[45] Karimi-Maleh H, Biparva P, Hatami M. A novel carbon paste electrode based on NiO/CNTs nanocomposite and (9,10-dihydro-9,10-ethanoanthracene-11,12-dicarboximido)-4-ethylbenzene-1,2-diol as a mediator for simultaneous determination of cysteamine, nicotinamide adenine dinucleotide and folic acid. Biosens. Bioelectron. 2013;48:270–275. doi:10.1016/j.bios.2013.04.029

[46] Karimi-Maleh H, Tahernejad-Javazmi F, Atar N, Lutfi M, Gupta VK, Ensafi AA. A novel DNA biosensor based on a pencil graphite electrode modified with polypyrrole/functionlized multiwalled carbon nanotubes for determination of 6-mercaptopurine anticancer drug. 2015;54:3634–3639. doi:10.1021/ie504438z

[47] Moradi R, Sebt SA, Karimi-Maleh H, Sadeghi Roya, Karimi F, Bahari A, Arabi H. Synthesis and application of FePt/CNTs nanocomposite as a sensor and novel amide ligand as a mediator for simultaneous determination of glutathione, nicotinamide adenine dinucleotide and tryptophan. Phys. Chem. Chem. Phys. 2013;15:5888-5897 DOI: 10.1039/C3CP00033H

[48] Fujimori A, Yamato R, Kikkawa T, Tatewaki Y. Morphological Transition of a Conductive Molecular Organization with Non-covalent from Nanonetwork to Nanofiber. J. Colloid Interf. Sci. 2015;448:180–188. doi:10.1016/j.jcis.2015.02.024

[49] Fujimori A, Arai S, Kusaka J, Kubota M, Kurosaka K. Formation and Structure of Langmuir–Blodgett Films of Organo-modified Alminosilicate with High Surface Coverage. J. Colloid Interf. Sci. 2013;392:256–265. doi:10.1016/j.jcis.2012.08.075

[50] Fujimori A, Kusaka J, Nomura R. Formation and Structure of Organized Molecular Films for Organo-modified Montmorillonite and Mixed Monolayer Behavior with Poly(L-lactide). Polym. Eng. Sci. 2011;51:1099–1107. doi:10.1002/pen.21912